ABSTRACT

Title of Document: SEPARATION OF FINE LIQUID DROPLETS
                      FROM HIGH SPEED AIR UTILIZING THE
                      ELECTROHYDRODYNAMICS TECHNIQUE

                      Ning Yang, Mater of Science, 2015

Directed By: Professor Michael Ohadi, Mechanical Engineering

With constant process intensification in recent years, the separation of fine micron and submicron size liquid droplets from gaseous flow mediums has become an important subject for the process and aerospace industries. While conventional technologies are not effective in this droplet size range, electrostatic separation demonstrated remarkable effectiveness and reliability while lowering maintenance and operation cost. However, it is commonly used for low droplet concentration in relatively low velocity gas flow. This current experimental study is focused on electrostatic separation of high concentration of fine electrically conductive droplets from high velocity gas flow. Different separators including wire-to-plate, wire-to-cylinder, single stage, and multi-stage separators were designed, built and tested at gas velocities up to 15 m/sec and droplet concentration up to 22,000 ppm. The results demonstrated that two-stage plate, as well as tubular separators provides maximum separation efficiency at minimum power consumption. However, the tubular separator is easier to package in the required space envelope and 1-inch diameter tubes are more efficient at high velocity and droplet concentrations.

SEPARATION OF FINE LIQUID DROPLETS FROM HIGH SPEED AIR UTILIZING
THE ELECTRODYDRDYANMICS TECHNIQUE

By

Ning Yang

Thesis submitted to the Faculty of the Graduate School of the
University of Maryland, College Park, in partial fulfillment
of the requirements for the degree of
Mater of Science
2015

Advisory Committee:
Professor Michael Ohadi, Chair
Associate Professor Gary A. Pertmer
Assistant Professor Siddhartha Das

Dedication

To my parents who have supported and encouraged me always.

Acknowledgements

First I would like to express my gratitude to my advisor Dr. Michael Ohadi and my mentors Dr. Amir

Shooshtari and Dr. Serguei Dessiatoun for the useful comments, remarks and engagement for completion

of my research. Without their guidance and persistent help this dissertation would not have been possible.

Finally, I would like to thank my friends at Smart and Small Thermal System Laboratory (S2TS) for

providing help and advices.

Table of Contents

List of Figures and Tables

Chapter 1: Introduction

1.1 Background

In this section the background and mechanism of electrostatic separator are reviewed. Then various particle generation methods including ultrasonic fog generator, fog machine, and nozzle are introduced and discussed.

1.1.1 Background of Electrostatic Separator

In recent years many industries have shown great interest in separation of fine droplets from gas stream. In the past, various traditional techniques were used to separate fine particles: some of them are cyclonic separation, gravity separation, and mechanical filtration. Unfortunately, the performances of most of these techniques are constrained by the particle size. As the size of particles reduces, these techniques become less efficient and separation process becomes more expensive. In order to separate micron and submicron size solid particles, electrostatic discharge technology has been employed. However, applications of this technology for separation of liquid droplets have not been explored extensively. The electrostatic separators are devices, which use electrostatic force to deflect and separate particles from a flowing gas. These separation devices have proven to be useful in industrial and residential applications. For example, it is used in power plant for separating of harmful particles from exhaust gas. It can also increase the reliability of operation by separating micron size corrosive liquid particles from a gas flow. The most common structure of electrostatic separator is a tubular geometry where a discharge electrode is placed at the centerline as shown in Figure 1.
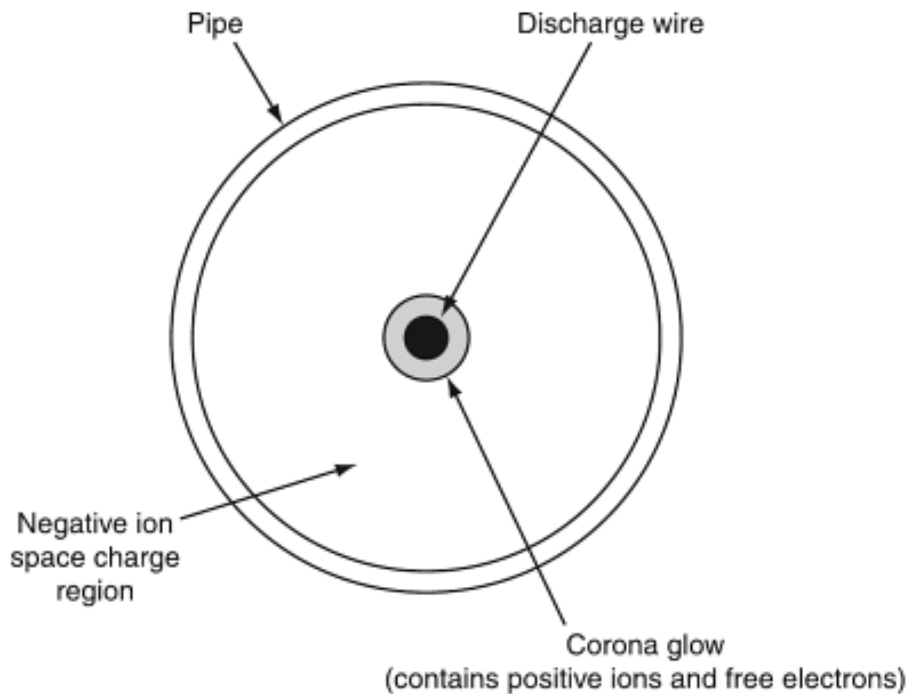
Figure 1: Schematic tubular separator arrangement [1]

The main advantage of an electrostatic separator, as compared to other separators, is its ability to separate micron-size particles with high collection efficiency. High collection efficiency may also be obtained by using mechanical filtration. However, for separation of micron-size droplets the pressure drop penalty of this method can be very high. On the other hand, electrostatic separator can separate particles by using electrostatic force and without any significant pressure drop. It also demonstrates high reliability and low maintenance cost.

1.1.2 Separation Mechanism

Figure 2 graphically summarizes the collection mechanism of a typical wire-to-tube electrostatic separator. The figure is a quarter sectional view of the separator. As it can be seen, the space between high voltage charged electrode and the ground electrode can be divided into two zones: active zones and passive zones.
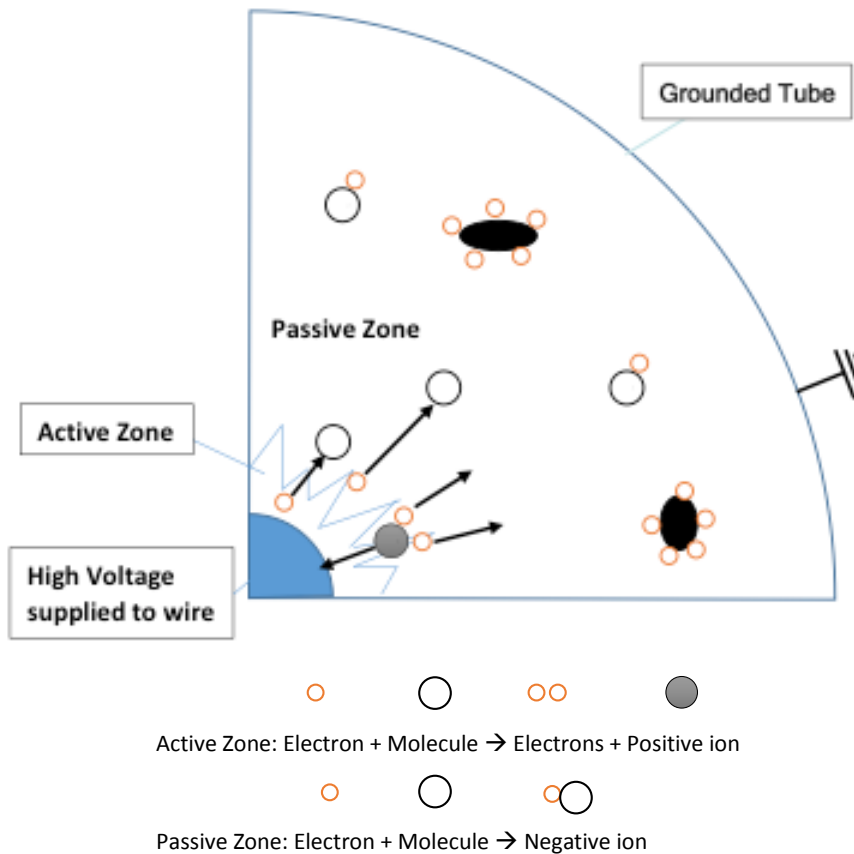
Figure 2: Collection mechanism in a wire-to-tube electrostatic separator with negative charged wire and grounded tube

Ionization process takes place in the active zone. By charging the wire electrode with high voltage (negative voltage in this case), the space in vicinity of the wire is ionized leading to production of large amount of high-speed electrons. The electric field created between the charged wire and grounded tube tends to derive the electrons towards the tube. On their way, the high-speed electrons may hit the gas molecules. This process doubles the amount of generated electrons and creates positive ions. Positive ions are absorbed towards the negatively charged wire. Electrons will migrate to the grounded tube.

As the electrons move further into the passive zones, due to a lower electric field, their speed is lowered down. No further ionization process occurs in this region and electrons are able to attach

to the moving particles. The grounded tube collects negatively charged particles. Separation process of particles is now completed.

During particle charging process, depending on the particle size, two different charging mechanisms may come into play, which is diffusion charging and field charging. The diffusion charging is caused by random collisions of ions with particles due to temperature (The Brownian motion) as described by gas theory. This mechanism is typically the prevailing charging mechanism for particles smaller than 0.2 μm. For particles larger than 1 μm, the field charging is the major charging mechanism. Field charging requires the presence of an electric field to drive the free mobile charge carriers. For particle sizes fall in 0.2 - 1 μm range combination of two charging mechanisms will be in effect. [1]

In terms of physical structure, there are two general types of electrostatic separators as shown in Figure 3. Figure 3(a) shows a plate-type separator (also known as planar separator), which is composed of two stages: charging stage and collection stage. The charging stage is positioned at the entrance of the system. High intensity electrostatic field is generated in this region by applying high voltage to a negatively charged wires positioned between the grounded plates. Particles are charged with a negative polarity at the charging stage. The collection stage consists of parallel plates. Every other plate is connected to the positive polarity while the plates in between are grounded. The applied electric field of the collection stage, although it is not as intense as the charging stage, is able to attract negative charged particles and complete the collection process.

Figure 3 (b) is a schematic sketch of the cylinder-type separator (also known as tubular separator). Compared to the plate-type separator, the structure is simpler. It consists of a charging wire electrode and a grounded tubular electrode. The wire is often charged with a negative polarity placed in the center of tube. Particles moving along the tube are charged negatively in

4

vicinity of the wire and move towards the ground electrode (i.e. tube) as a result of the electric field. If the device is used for separation of liquid droplets, a stream of liquid can be formed at the bottom of tube as the process of collection of droplets continues. Collected liquid must be discharged through a drainage system.
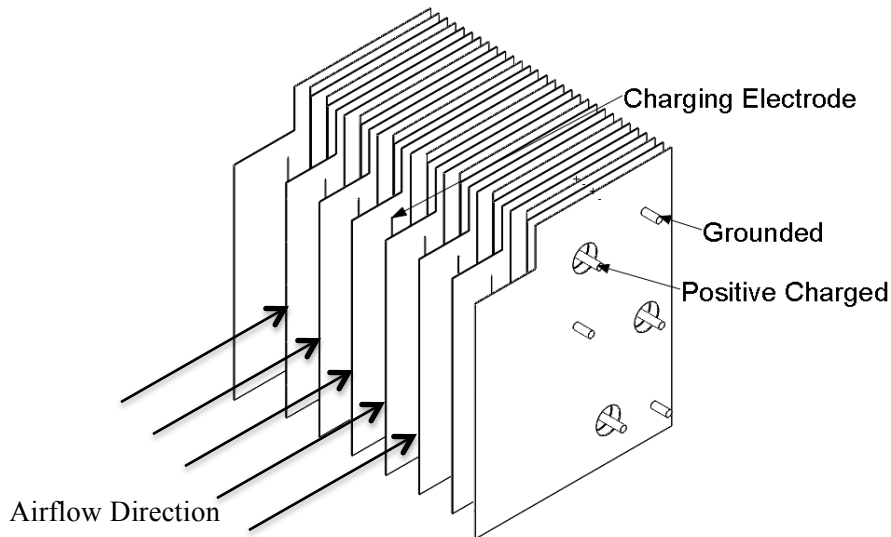
(a) Sketch of planar electrostatic separator
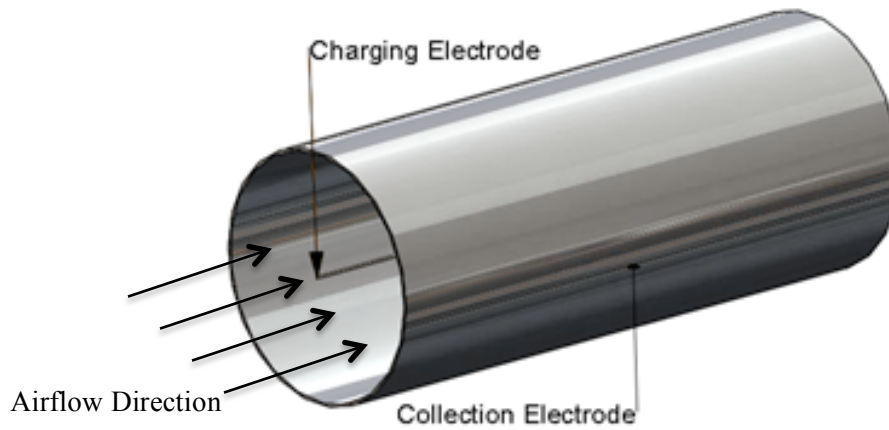
(b) Sketch of cylindrical electrostatic separator

Figure 3: Sketch of electrostatic separators: (a) sketch of planar electrostatic separator, (b) sketch of cylindrical electrostatic separator

1.1.3 Particle Generation Techniques

There are a number of techniques that can be used to produce high concentration of small size droplets. A review summary of the important techniques is given in this section.

1.1.3.1 Ultrasonic Fog Generator

Ultrasonic fog generator, which is also known as ultrasonic humidifier, is one of the methods of producing liquid droplets. Figure 4 shows a multiunit ultrasonic fog generator. Ultrasonic fog generator uses a piezoelectric transducer to create a high frequency mechanical oscillation in a film of water. Metal diaphragms vibrate at this high ultrasonic frequency to create small water droplets that exit the system silently.

Figure 4: Ultrasonic fog generator

It was shown that the size of the micro water droplets can be manipulated by adjusting the driving frequency. An increased driving frequency leads to a smaller mean droplet diameter. Boucher and Kreuter describe a droplet formation expression derived by Lang and refined by Penskin and Raco [2]. The expression depicts the median aerodynamic diameter of aerosol droplets produced by an ultrasonic humidifier for a given liquid surface tension and piezoelectric crystal operating frequency as given by Eq. 1.

$$D_{Ndrop} = 0.34(8\pi S/(\rho_{liq}F^2))^{1/3} \qquad\qquad (1)$$

where D_N is number median droplet diameter; S is liquid surface tension; ρ is liquid density; F is crystal frequency

For a specific liquid, the surface tension and the density are constant. Hence, the droplets size is inversely correlated with the diaphragm vibrating frequency. It was reported that a humidifier with a 1.6 MHz transducer produces droplets with a number median diameter of 3 μm [3] .

1.1.3.2 Fog Machine

Fog machine is a device that uses a heating element to emit a dense vaporized fog. A picture of this machine is shown in Figure 5.

Figure 5: Fog machine

Typically aqueous glycols and mineral oil (sometimes called fog juice) are used to produce small droplets in a form of dense fog. [4] Fluid vaporizes inside fog machine through a heat element. Then the vaporized fluid is injected to the environment and as result of a contact with moisture in air, a thick visible fog is generated.

2.2.3 Nozzle

Nozzle is a device that facilitates dispersion of liquid into atomized form. Figure 6 shows specific kind of nozzle used in current study to produce water droplets.

Figure 6: Nozzles

The size of droplets is influenced by some factors, including nozzle geometry, injection pressure, and liquid characteristics [5] [6] [7]. Figure 7 demonstrates the relationship between particle size and injection pressure. It can be seen that by increasing the injection pressure, smaller particle can be produced by nozzle.
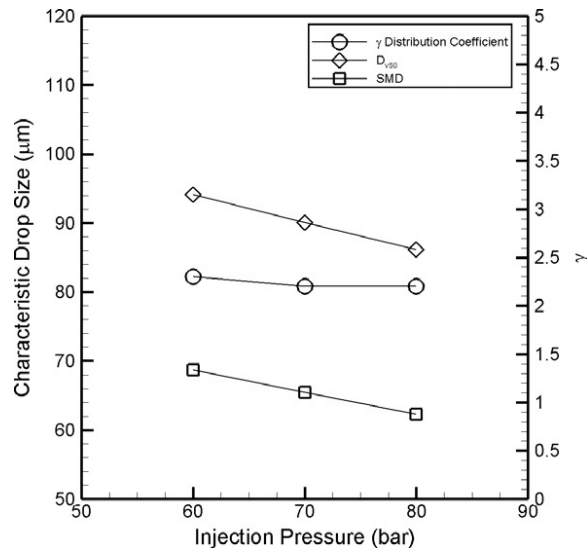
Figure 7: Trend of droplet size versus operative pressure [6]

The current study focuses on development of electrostatic separators for separation of fine liquid droplets from a high-speed air stream. Several factors are studied to enhance the performance of the separator. The particle size plays an important role in separation performance. Theoretically, electrostatic separator can collect particles with diameters as low as 0.01 μm up to 10 um and higher. To further study the effect of particle, a numerical study is performed to investigate the effect of this factor on the collection efficiency. The amount of the charge accumulated on a given particle is calculated and the trajectory of the particle under the influence of the electric field is determined.

Airflow rates also influences the efficiency of the electrostatic separator. As the airflow rate increases, it reduces the residence time of the particles inside the separator. If the airflow rate is too high, it is likely that there is not sufficient time for a particle to reach to its charging saturation state. If the airflow rate is too low, the full collection may happen within a short portion of separator and the remaining section is not properly utilized. This can lead to wasting of the electrical power supplied to the separator. Hence, there is a direct relationship between the air velocity and the optimum size of the electrostatic separator. This is another factor to be investigated in current study.

For the wire-to-tube designs, diameter of the tube is an important factor. As the diameter of the tube decreases, higher electrical field is produced due to a shorter distance between charging and collection electrodes. However, if the diameter is kept constant and instead a higher voltage is applied to increase the electric filed, the plasma region doesn't grow proportionally. It means that for a same average electric field between two electrodes the extent of plasma region of larger diameter is smaller than that of the smaller diameter. Since the amount of particle being charged depends on the size of the plasma region, a relative larger portion of plasma region will result in higher collection efficiency. However, reducing the diameter and decreasing the distance between

9

two electrodes can result in an early spark over. The effect of the diameter is another subject that will be investigated in current study.

It is observed that in a flat plate electrostatic operator a two-stage configuration can produce higher collection efficiency than a single-stage configuration. Therefore, as part of the current effort, the concept of two-stage configuration was extended to a tube design as well. Then the ratio of charging stage length to the total length of tube was investigated experimentally. It is observed that when the length of charging stage is too short, it leads to insufficient charging of particles and a drop in collection efficiency. On the other hand, if the charging stage takes up too much length it will also result in a deficiency of performance of electrostatic separator due to an insufficiency in particles collection. This resulted in determining an optimum for the length of charging stage.

1.3 Research Objectives and Approach

The main objective of this study is to develop an electrostatic separator prototype, which is able to achieve the collection efficiency over 90% when separating fine water particles in high velocity airflow. Meanwhile, the power consumption should be minimized.

The details of test condition requirements are summarized in Table 1.

Table 1: Test condition requirements

Variables	Range
Air Velocity	≈ 10 m/s
Droplets Concentration	≈ 22 g water/kg air
Mean Droplets Size	≈ 1.7 µm
Physical Envelope	≈ 6.5" x 24"
Efficiency	Over 90%

In order to accomplish the main objective of this study, the test condition needs to be created and the performance of the separator for different design alternatives to be studied. Constant airflow velocity is obtained by utilizing an air blower in conjunction with a variable transformer. The required droplet size and concentration is achieved by mixing the particles produced by two different kinds of particle generators, fog machine and ultrasonic fog generator.

1.4 Dissertation Organization

The outline of this thesis is as follow: Chapter 2 of the thesis provides a survey of the literature and a summary of the relevant studies. Chapter 3 discusses a numerical study to improve the understanding about the effect of various parameters of electrostatic separator including electric field, applied voltage, charging density, particle size, diameter, and length on trajectory of particles and separation performance. Reviews of experimental studies are presented in chapters 4 and 5. Chapter 4 provides a review of experimental setup and test designs for both wire-tube and wire-plate separators. In chapter 5, an improved separator design is introduced and the results of study on certain performance influencing factors are discussed. These factors include the airflow velocity and diameter size of tube. A comparison of the results among different designs and the final prototype design are presented in this chapter as well. Chapter 6 discusses the fabricated full-scale prototype and the corresponding experimental results. Conclusions and proposed future work are discussed in chapter 7 of the thesis.

Chapter 2: Literature Study

The use of electrostatic discharge to remove particles from gas stream was first introduced in1824 by Hohlfeld [8]. However, it was not fully studied until 1907, when the first device was invented by Frederick G. Cottrell, a professor of chemistry at the University of California, Berkeley [9]. Since then, electrostatic separators have been researched extensively due to its high separation performance and low energy consumption. However, the focus of major previous works has been on solid particles, and separation of droplets has not been investigated thoroughly. Some of the earlier works related to the electrostatic separator will be discussed in this section.

Yi et al. have carried out experimental studies on a self-designed, plate type electrostatic separator and conducted a parameter study on ion concentration, the distance between collection plates, and the particle velocity. They showed that the gas ion concentration can be enhanced 1-2 magnitudes by increasing the particle velocity due to the prevention effect of gas ion neutralization. Therefore, collection efficiency can be increased [10].

Bologa et al. conducted an experimental study on the influence of aerosol temperatures on the characteristics of corona discharge particle size distribution. The experiment was based on the principle of unipolar particle charging in corona discharge to collect fine oil mists. The results indicated that the characteristics of corona discharge and particle size distribution will change with the increase of gas temperature [11].

Podlinshi et al. studied the influence of electrohydrodynamic secondary flow on the collection efficiency of electrostatic separators with positive and negative voltage polarity. A spike tip discharge electrode was experimented with in the study. By directing the tip either upstream or downstream the primary flow, while keeping other parameters constant, the flow pattern and

efficiency changes. The results indicated that the secondary flow is the main reason that the collection efficiency of the separator changes [12].

McKinney et al. designed a barbed plate electrostatic separator to generate a more uniform current density distribution and electric field. The results of the device were compared to a wire-plate separator by measuring the particle motion via a laser Doppler velocimeter. The flow pattern indicated that the barbed plate separator shows a more uniformly distributed current density and electric field. Also the plate type separator creates large-scale, secondary flows during separation process [13].

Grass et al. conducted an experimental work on the influence of different electrical fields and properties on the electrostatic separator, and the power consumption of different high voltage supplies. They discovered that different high voltage supplies show different electrical properties and efficiency. The results from the experiments demonstrated that increased efficiency for large particle sizes and high particle concentrations can be achieved with high frequency power supplies. Alternatively, more efficient separation can be obtained for fine particles with pulsed power supplies. In addition, experiments on power consumption showed that a high frequency IGBT inverter combined with a /spl mu/s-pulsed power supply can improve the overall separator performance [14].

Dumitran et al. experimentally studied the drift velocity of fine particles. A laboratory-scale, two-stage separator was first designed. The ionization process is achieved with barbed electrodes. The collection stage is maintained with uniform electric field. Results of separation efficiency for different values of turbulent diffusivity can be derived to obtain the drift velocity. In addition, the influence of gas flow turbulence was studied with experimental data [15].

Touhami et al. conducted a numerical simulation on the trajectory of insulated particles. It was indicated that the trajectory of the particle movement can be precisely determined with numerical

simulations based on the equation of the forces exerted on the particle in the electrical field. The electric field was simulated with COMSOL software. The trajectories of electrically charged, insulating particles were simulated with MATLAB to study the factors that influence the process of selective sorting of various granular materials [16].

Rajanikanth et al. performed an electric field simulation in order to predict the physical processes of a plate-wire electrostatic separator in the prebreakdown region. The simulation can be used to predict the voltage current characteristics, which further help to diagnose the electrical problems. It was shown that the simulation results were validated against the experimental results [17].

Lancereau et al. conducted a numerical work to identify dimensionless numbers dictating the electrohydrodynamic transport in the tube-wire electrostatic separator under laminar flow conditions. The dimensionless numbers are, except for two geometrical parameters, the electric Reynolds number Re_e, the hydrodynamic Reynolds number Re_a, and the ratio between the peek field and the mean electric field between the two electrodes. The results indicated that the four regimes in the separator are limited by the length of electrode. A basis was provided with the simulation to study the influence of the secondary flow on the performance of electrostatic separators [18].

Zhi-jiang et al. did an experiment to study the V-I characteristics. Based on the characteristics, the performance of separators can be improved. The influence of different gas velocities, droplet sizes, and droplet concentrations has been studied. It was shown that, at a gas velocity of $1.0 \sim 1.2$ m/s, a nozzle pressure of $0.3 \sim 0.4$ MPa, and a volume flow rate of water $0.24 m^3/h$, the optimized efficiency can be achieved [19].

Chua et al. experimentally studied the micro-fabricated electrostatic separator. Poly-dispersed liquid phase oleic acid particles, with sizes ranging from 20nm to 300nm, were utilized in the experiments. The separator designed had an electrode gap of 1.8 mm to 2.0 mm, and tested at

2.2kV and 2.6kV, respectively. The experiment's results were both detected by visual observation and the measurement of the corona current during the separating process. It was demonstrated that the micro-fabricated electrostatic separator sufficiently separated the micron-sized particles [20].

Yamamoto et al. developed a design of an electrostatic separator which can not only separate low resistive particles, but can also incinerate captured particulates, which all generated from diesel engine. The device utilized ionic wind to carry the charged particles to the passive zone, where the repulsion force exerted on the particles is much smaller than active zone. Therefore, the re-entrainment phenomenon can be suppressed. Meanwhile the captured particulates will be incinerated by ozone and other oxidation products. The separator was first designed by optimizing the electrode location. Then the experiment's results were detected by scanning mobility particle sizes and the particle counter. The new separator design demonstrated the potential of diesel engine emission control [21].

Zukeran et al. experimentally investigated the reason that the electrostatic separator shows low collection efficiency. Both the collection efficiency and the particle size distribution were studied. The results demonstrated that the decrease in collection efficiency was caused by subsequent release of the particles into the atmosphere during separator operation. Then the influence of the airflow velocity on the re-entrainment effect was studied. It was shown that the re-entrainment phenomenon is dependent on the airflow velocity [22].

Schwab also conducted an experimental study on the back corona behavior. Particles with high resistivity were collected in a laboratory scale, electrostatic separator. The results indicated that the high resistivity particles will lead to the occurrence of back corona, which decreases separator collection efficiency. Since the local occurrence is related with dust layer thickness and the porosity, which is affected by the electrohydrodynamic field, the electric current density's

increase was monitored. The study demonstrated the existence of different types of back corona. Also, it showed the relationship between the quality of the dust layer and the occurrence of back corona [23].

Wang et al. conducted experimental and numerical studies on the effect of negative corona discharge of the electrostatic separator. The current voltage characteristics were measured experimentally for a range of temperatures and relative humidity and the influence of humidity on the electric field and charge density was numerically studied. The results demonstrated that the inception voltage and electric field decreased with the increase of humidity [24].

Chang et al. conducted an experiment that studied the particle image velocimetry measurements of the flow velocity field in a wire-tube electrostatic separator. The voltage supplied to the separator has negative polarity. The influences of Reynolds and electrohydrodynamic numbers on the system collection efficiency were investigated. It was shown that when the $Ehd/Re^2 >= 1$ and $ReSc >= Fe$, where Sc is the Schmidt number and Fe is the electric field number; the separator collection efficiency is affected by the electrohydrodynamic secondary flow [25].

Blejan et al. measured the collection efficiency for three different cylindrical electrostatic separator designs to improve separator performance. The different diameters of the collection electrodes of separators were fabricated and tested. Current voltage characteristics were first compared with standard electrode arrangements. Then the results of second experiments demonstrated the relationship between current density distribution and the geometry of the electrode system. Dust collection efficiency was measured in the third set of experiments. The results showed that the modified separator demonstrates higher collection efficiency compared with the standard design. It is also shown that the lower collection efficiency occurs at higher flow velocity [26].

Mizuno described the principles of electrode separators, including particle charging, migration velocity of charged particles, and collection efficiency. Abnormal phenomena were also described, including back corona for treating high resistivity dust, abnormal re-entrainment for low resistivity dust, and corona quenching for fine dusts. Techniques to solve these abnormal phenomena were also introduced. Pulsed energization separators can remove high resistivity dusts and lower power consumption. Wet electrostatic separators are able to remove dusts and gaseous pollutions simultaneously. Some applications were also included which can remove dioxin from incinerators [27].

From this literate survey it can be concluded that the focus of previous works has been mainly on separation of solid particles. The influences of some influencing parameters have been studied to investigate the performance of electrostatic separator. However, there has not been a systematic study on separation of fine droplets from high-speed gas stream and drainage of collected liquid. This thesis will focus on the study of separation of these droplets and methods to improve the system efficiency.

Chapter 3: Theoretical Modeling

3.1 Introduction

In section 1.2, the background and concepts of electrostatic separators were described. The process of generation of ions, their motion in the electric filed and attachment to particles and deflecting particles trajectory is a complicated physical phenomenon. As explained in Section 1.3, the performance of a separator can be mainly characterized by its electric field, current density, the voltage supplied to the system, and the particle size. In order to better understand the separation performance and identify the influence of design parameters, a numerical modeling effort has been conducted. This chapter describes the governing equations and numerical methodology used to calculate them.

3.2 Model Description

A simple geometry of tube-type separators consisting of a thin wire and a grounded tube will be considered and modeled using Engineering Equation Solver and Matlab.

The physical geometry is shown in Figure 8. The diameter of the charging wire is set to 0.22 mm. In this study the trajectory of a single particle under the influence of the electric field is to be modeled. Particles near the wire are the most difficult to collect, due to the longer distance to reach the grounded tube. Therefore, the initial location of the particle is selected very close to the charging wire (the distance to charging wire is 0.02 cm). The diameter of tube is 2.54 cm (1 inch). The length of electrostatic separator is 35 cm, determined by physical envelope constrains.
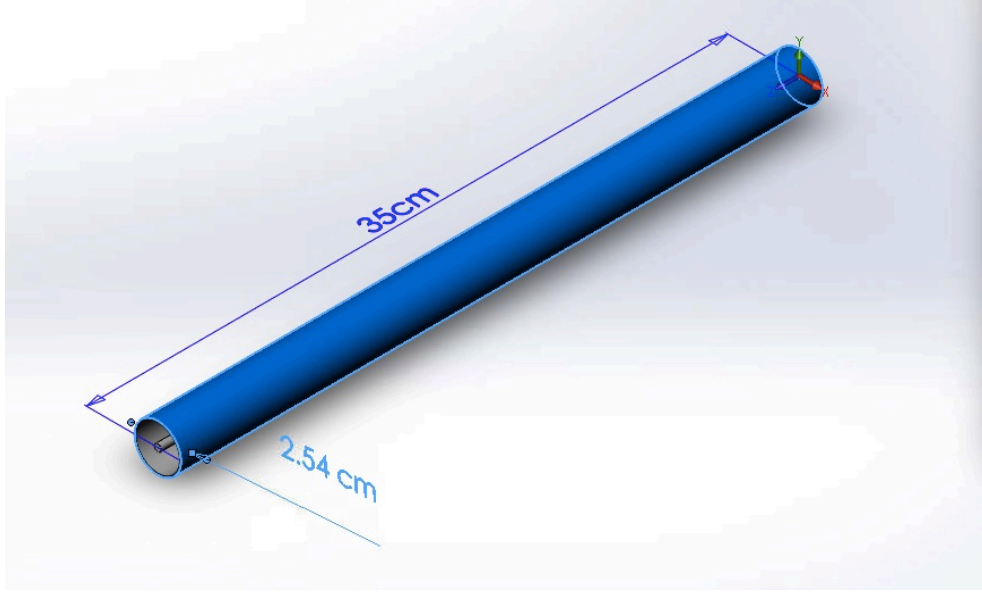
Figure 8: Physical geometry of separator

The trajectory of particles is simulated to study the collection length and the factors influencing the performance of separator, such as particle size, grounded tube diameter, different electric field. The trajectory can be determined from the momentum balance applied to a single particle.

$$\frac{d\mathbf{u_p}}{dt} = F_D\left(\mathbf{u} - \mathbf{u_p}\right) + \frac{\mathbf{g}(\rho_p - \rho)}{\rho_p} + \mathbf{F_e} \tag{2}$$

where $\mathbf{u}$ and $\mathbf{u_p}$ are the velocity of air flow and particle; ρ and ρ_p are the density of air flow and particle; F_D is Stokes drag term; $\mathbf{F_e}$ is electrostatic body force; t is resident time s.

The Stokes drag term is given as:

$$F_D = \frac{C_D R_e}{24} \frac{18\mu}{\rho_p d_p^2} \tag{3}$$

where C_D is the drag coefficient for sphere particles;

The last term in Eq.1 represents the electrostatic body force exerted on a charged aerosol, given as:

19

$$\mathbf{F_e} = \frac{q_p\mathbf{E}}{1/6\pi d_p^3 \rho_p} \qquad (4)$$

To calculate the electrostatic body force, the local electric field in vicinity of aerosol particle and the charge accumulated on the particle must be determined. The total particle charge is given as:

$$q_p = q_{diff} + q_{fld} \qquad (5)$$

The assumption is that only field charging happens during the whole separation process. It is reported that when the particle size is larger than 1 micron, the field charging is the dominant charging mechanism. Therefore, diffusion charging is neglected in the current simulation. To calculate the electrostatic body force exerted on a charged particle, the amount of charge acquired by a particle due to field charging is given by [28]:

$$q_{field} = \left(\frac{3\varepsilon_p}{\varepsilon_p + 2}\right)\left(\frac{\mathbf{E}d_p^2}{4K_E}\right)\left(\frac{\pi K_E Z_i \rho_i t}{1 + \pi K_E Z_i \rho_i t}\right) \qquad (6)$$

where ε_p is relative permittivity of the particle; $\mathbf{E}$ is electric field strength; d_p is diameter of particle; K_E is proportionality constant ($9.0*10^9$ Nm^2/C^3); Z_i is ion mobility; ρ_i is charge density space.

The relation between potential and electric fields is given by

$$\mathbf{E} = -\nabla\emptyset \qquad (7)$$

where $\mathbf{E}$ is the electric field intensity; ϕ is potential field.

The current density is the summation of ionic mobility, conduction and convection components. However, since the electrical conductivity of air is negligible, the velocity of airflow can be neglect compared with the ion mobility. Therefore, the current density, $\mathbf{J}$, is given as:

$$\mathbf{J} = \rho_i Z_i \mathbf{E} \tag{8}$$

To calculate current voltage characteristics, the threshold field strength can be determined semi-empirically using Peek's formula (Eq. 8).

$$E_0 = 30\delta + 9\sqrt{\frac{2\delta}{d_w}} \tag{9}$$

where d_W is diameter of wire. δ is relative density;

$$\delta = \frac{T_0}{T}\frac{P}{P_0} \tag{10}$$

where T is actual fluid temperature; T_0 is absolute ambient temperature; P is actual fluid pressure; P_0 is normal atmosphere pressure.

At low voltages, due to the absence of ionization processes, the particle cannot be separated from the airflow. But when the voltage gradient around an electrode goes above the threshold value, the air surrounding can dissociate molecules into ions, which results in charging of moving particles and initiation of separation processes. In the numerical study, it is assumed that the maximum electric field is equal to threshold field.

The relationship between the threshold field strength and corona onset voltage given as

$$\emptyset_0 = \frac{d_w}{2} E_0 \log\left(\frac{d_c}{d_w}\right) \tag{11}$$

where E_0 is the initial field strength; d_c is cylinder diameter

21

3.3 Simulation Results and Discussion

The influence of several factors such as particle size, electric field, and current density on the collection efficiency is studied using a numerical simulation approach.

3.3.1 Study of Electrical Characteristics

Studies were conducted on electrical characteristics of the separator, namely, electric field and charge density in radial direction.

Figure 9 shows variation of the electric field along a radial distance (r) within the tube. The result indicates a decreasing trend along with the increasing distance in the radius direction. Close to the center of tube and approximately 0.002m away, the electric field drops dramatically with increasing distance to the center. As it extends further away from the center, electric field declines gradually to a relatively flat curve. This characteristic further explains Figure 2. In the active zone, the electric field is rather high, where corona discharge occurs, large amount of electrons are generated in this region. When the electrons travel further away from the center, the electric field is relatively low, and no more ionization processes occur. Electrons are able to attach the particles. Then, the grounded collection tube can collect the negatively charged particles.
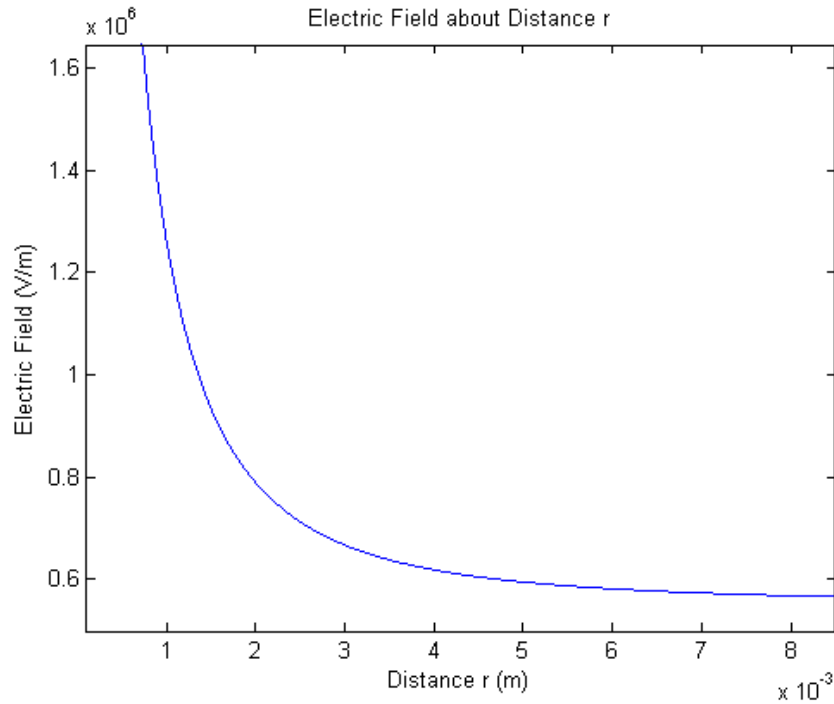
Figure 9: Electric field about distance r

Charge density variation with the distance along the radius direction (r) is shown in Figure 10. Charge density indicates the amount of electric charge per unit volume, which is directly related to the amount of charge accumulated on a moving particle. Increasing the amount of charge accumulated on moving particles will result in higher collection efficiency. The particles receive larger amount of charge near the charging electrode. When a particle travels further away from the charging electrode, the likelihood of being charged decreases.
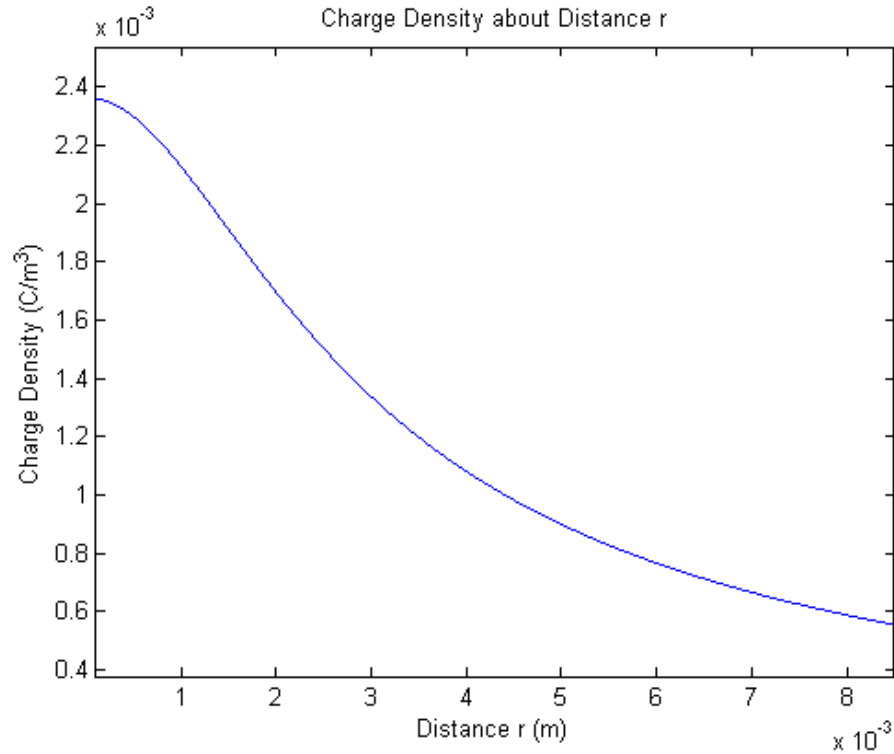
Figure 10: Charge density about distance r

3.3.2 Study of Particle Size Effect

Particle size is an important influential factor for separator performance. As discussed in chapter

1.2, there is a certain range of particle sizes where the separator shows lower collection efficiency.

Since the focus of the current modeling is on the field charging, the collection effect only for

particles larger than 1 μm is simulated. For particles smaller than 1 μm the effect of diffusion

charging becomes important and the current modeling results may not be accurate any more. It

should be noted that the average size of droplets per project requirements is approximately 1.7

μm.

The result of the particle sizes influence on performance is shown in Figure 11. The trajectory of

different particle sizes is modeled to interpret collection efficiency. As the diameter of tube is

selected to be 1 inch (2.54 cm), the initial position of particles is near the center, approximately

0.5 inch (1.27 cm). X-axis coordinates can be seen as tube wall. The line parallel to the x-axis at

24

the initial position of the particle can be considered to be the center charging wire. There are two

competing forces actin on a given particle: the drag force, which is pushing the particles along the

length of the tube, and electrostatic force, which force the particle to move radially. If the

trajectory of a particle intersects x-axis coordinate, it can be identified as collected by the

separator. Trajectory of 10 μm particle, for instance, shown in the red line, passes x-axis at

approximately 9 cm. It indicates that 10 μm particles can be separated at 9 cm. Therefore, the

separator shows high performance when collecting particle sizes of 10 μm. As the size of the

particles reduces the separation process becomes more difficult. However, it must be noted that

for 1 μm particles and smaller the diffusion charging will also contribute in particle charging

process which has not been considered in current modeling effort. Therefore, there is a possibility

that those particles are still collected with adopting a slightly longer separation tube.
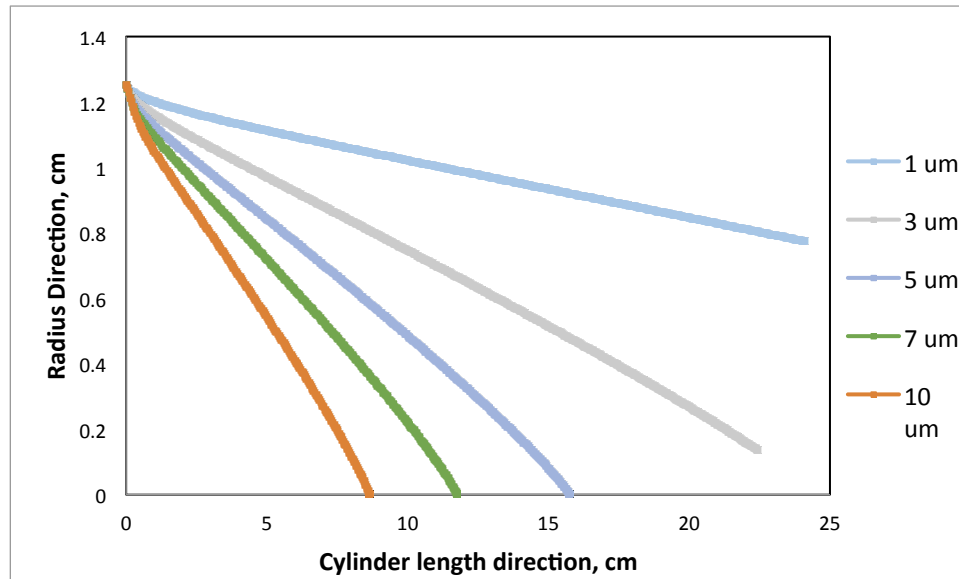
Figure 11: Trajectory of different particle size

3.3.3 Study of Collection Efficiency and Current Voltage Characteristics

It is also essential to investigate the collection efficiency corresponding to different voltages

supplied to the separator. Collection efficiency is determined based on the ratio of the particles

collected according to the trajectory of the particles and the total particles injected uniformly

across the entrance area of the tube. Particles of 3-micron diameter are simulated in this study. This calculation is based on the assumption that the particles discharge into the system uniformly.

The electric field, current density, and efficiency are obtained from the simulation, shown in Figure 12. It can be seen that the onset voltage for the separator is approximately 6.5 kV, which means that corona effects start to occur as voltage increases beyond this point. When the voltage is lower than the onset voltage, no corona effects take place, which indicates that the current density is maintained at a relatively low value insufficient to initiate the ionization process. After the onset voltage, current density gradually increases.

Figure 12 also reflects the relationship between collection efficiency and voltage. The general increasing trend of efficiency corresponds to the current voltage characteristics. When voltage is lower than onset voltage, that is, no corona effect in the system, the separator shows barely any collection. With the increasing voltage, efficiency increases dramatically and reaches 100% at 8.5 kV.
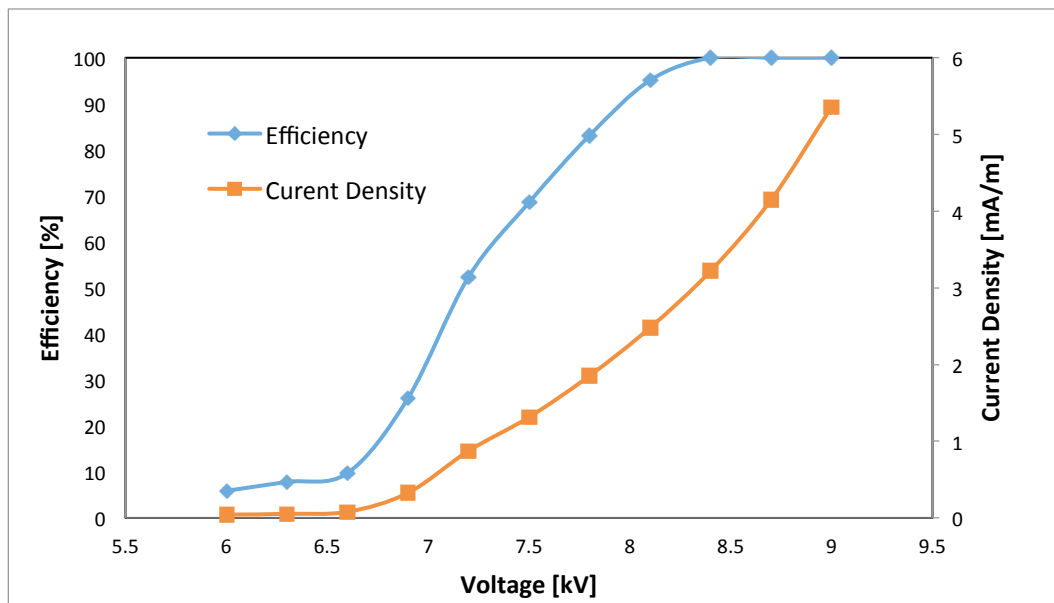
Figure 12: Current density and collection efficiency vs. voltage supplied

3.4 Summery

A model of the wire-tube separator is simulated to further study the parameters affecting the

separator performance. A description of the model and governing equations was presented in this

chapter. Electrical characteristics, the effects of particle size, current voltage characteristics on

collection efficiency were studied using this modeling approach. The model qualitatively shows

that the electric field and charge density are relatively high around the charging wire, and then

gradually decrease along the radius direction towards the grounded wall. It was observed that it is

more challenging to collect small droplets as opposed to large ones especially if these droplets are

entering the separator in vicinity of the centerline electrode. In order to obtain certain range of

collection, the voltage supplied to the system should be at least higher than the onset voltage.

Then, with increasing voltage, collection efficiency increases dramatically, and theoretically

reaches 100%.

Chapter 4: Electrostatic Separator Experiments

4.1 Introduction

In order to further study the performance of electrostatic separator, test setups for both wire-plate and wire-tube separators were designed and fabricated. For the plate type separator, different separator conditions were experimented to compare the difference between single stage and two-stage systems. As for the wire-tube separator, both the influencing factors of the separator and various electrode designs were tested to study the electrostatic separator characteristics and improve the collection efficiency, as well as lower the power consumption.

4.2 Wire-to-Plate Separator

Test setups for wire-to-plate and wire-to-cylinder separators are designed based on the respective configurations. However, they all consist of five main components: fog-supply system, air-supply system, electronic system, measurement unit, and the separator demonstration unit.

Table 2 shows the equipment used during the experiments. It also indicates the range and accuracy of specific equipment.

Table 2: Equipment measure range and accuracy

Name	Range	Accuracy
Opacity meter	0- 100 %	± 1.0 %
Aerodynamic Particle Sizer Spectrometer	0.5 μm – 20 μm	± 10%
Anemometer	0.30 m/s – 45.00 m/s	± 3%
Multimeter -Voltage	0 – 1000 V	± 0.05%
Multimeter -Current	0 – 10A	± 0.2%

4.2.1 Wire-to-Plates Separator Test Setup

Two separators are placed in a series to enhance separation efficiency. Each separator has a charging stage and collection stage as shown in Figure 13. When droplets flow through the separator, they are ionized and collected twice. Therefore, higher separation capability can be achieved.

Figure 13: Geometry of wire-to-plate separator

Figure 14 presents the setup for wire-to-plate separator, including the actual and schematic sketch of experiment configuration. The setup consists of fog machine, mixing channel, plate separator, high voltage power supply, opacity meter, and fan.

Before starting an experiment, airflow velocity will be measured at the system inlet, using anemometer to ensure sufficient flow rate. The fog machine is located at the system inlet. It generates a consistent amount of fog and injects it into the system. Air and fog particles are get mixed and become uniform in the mixing chamber. Charging and separation process occur in the electrostatic separator. High voltage power supplies provide high voltage to the separator, which is not shown in the figure. An opacity meter is set below the separator outlet to measure the

optical properties of gas. The opacity meters detect and measure the amount of light blocked by fog droplets remaining in the airflow after the separator, which is an indication of the separator performance. The fan, located at the system outlet, provides enough airflow speed to meet the test condition requirements. Variable transformer regulates velocity of the fan.
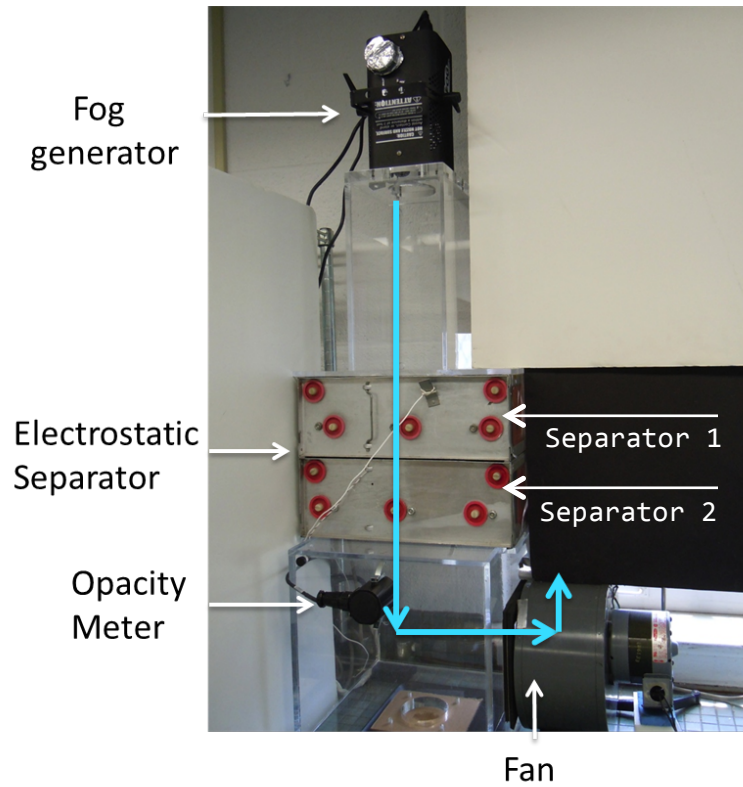
(a) *Wire-to-plate separator experiment setup*
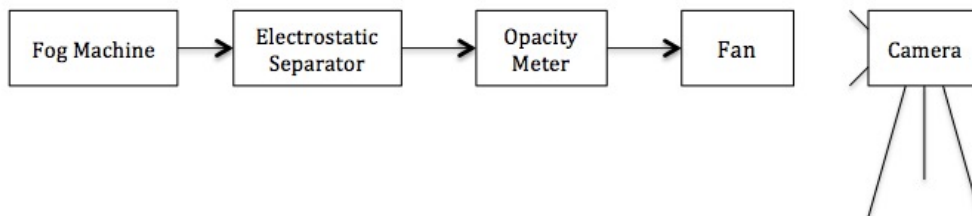
(b) Experiment setup schematic sketch of wire-to-plate separator

Figure 14: Experiment setup for wire-to-plate electrostatic separator: (a) wire-to-plate separator experiment setup; (b) experiment setup sketch of wire-to-plate separator

Figure 15 shows a close-up photograph of the opacity meter lens. After a few tests, it was observed that droplets accumulate on the opacity meter lens, which will influence the accuracy of the experiments. Therefore, a local stream of airflow was designed to keep away the fog from accumulating on the lens. The green pipe shown in the figure is used to provide a continuous small airflow stream.

Figure 15: Design used to prevent accumulation of liquid on opacity meter lens

Opacity is a measure of impenetrability to light, which can measure of the visibility of fog particles in the airflow. High opacity reading indicates that airflow contains high amounts of particles. Conversely, when the opacity reading is low after separation, it shows that the amount of particles remained is low, therefore demonstrates high separation performance. Hence, collection efficiency can be calculated by the ratio of opacity before and after separation as shown in Eq. 12. When no power is supplied to the separator, no separation process occurs. The opacity indicates the amount of particles before separation. By providing power to the separator, opacity is measured equivalent to the number of particles after separation process.

$$Efficiency = 1 - \frac{Opacity\ Reading\ with\ Power}{Opacity\ Reading\ without\ Power} \qquad (12)$$

4.2.2 Wire-to-Plate Separator Experiments

For wire-to-plate separators, four different conditions of separators were studied, which are "no charge", "one stage", "one charged wire", "two stage". As two plate separators are placed in the series, the upper separator is named separator 1. The other is labeled as separator 2.

"No charge" refers to the case where no power is provided to both separators. It is used as a reference case to identify the performance of other separator conditions. "One stage" refers to the case where only the charging stages of both separators are provided with power, which functions as two single-stage separators. Experiments of "one stage" separators are used to observe the difference between one-stage and two-stage separator. "One charged wire" and "two stage" are both two-stage conditions. However, the difference is that, for "one charged wire", only the charging stage of upper separator is provided with power. Particles will be ironized once and then move into the collection stages of both separators. For "two stage", particles, after passing through the charging stage of separator 1, can be charged again within the separator 2.

For the four conditions, variant voltage is supplied to the charging stage of the separator to study the separator performance. The voltage supplied to collection stage is kept constant at positive 4.8kV. It ensures that the negatively charged particles are attracted and attached to collection plate.

4.3 Wire-to-Tube Separator

4.3.1 Test Setup

The experimental setup for the wire-to-tube separator is shown in Figure 16. The setup consists of a fan, a fog generator machine, a water pump, a high voltage a power supply, and an electrostatic separator.

Table 3 shows the equipment used during the experiments. It also indicates the range and accuracy of specific equipment.

Table 3: Equipment measure range and accuracy

Name	Range	Accuracy
Regulated cylinder	0- 100 ml	± 1ml
Thermocouple	-200 °C- 350 °C	± 0.5 °C
Scale	0 - 20,000 g	± 0.1g
Aerodynamic Particle Sizer Spectrometer	0.5 μm – 20 μm	± 10%
Anemometer	0.30 m/s – 45.00 m/s	± 3%
Multimeter -Voltage	0 – 1000 V	± 0.05%
Multimeter -Current	0 – 10A	± 0.2%

As shown in Figure 16, airflow is blown into the system through a regulated fan, which is not shown in the figure. To ensure sufficient airflow supplied by the fan, the airflow velocity will be measured at the outlet of separator. Airflow blown by the fan will first enter the chamber, and receive water droplets produced by ultrasonic fog generator. Fog juice particles, produced by fog machine, come into the system at the elbow tube. The mixture moves into the separator. Particle are separated and collected in the tube separator. The reason for using both the fog generator machine and the ultrasonic fog generator is to obtain the particles mean diameter such that it will be closer to the test requirements of 1.7 μm.
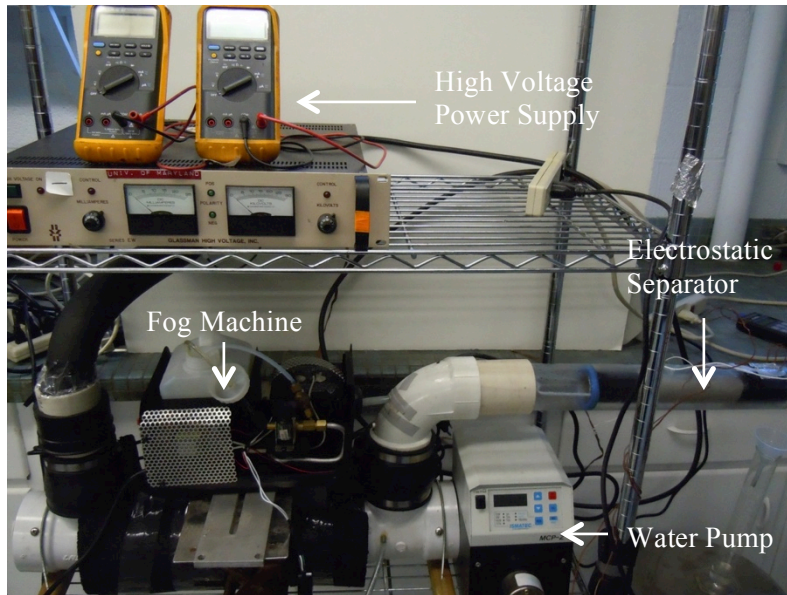
(a) Wire-to-tube separator experiment setup
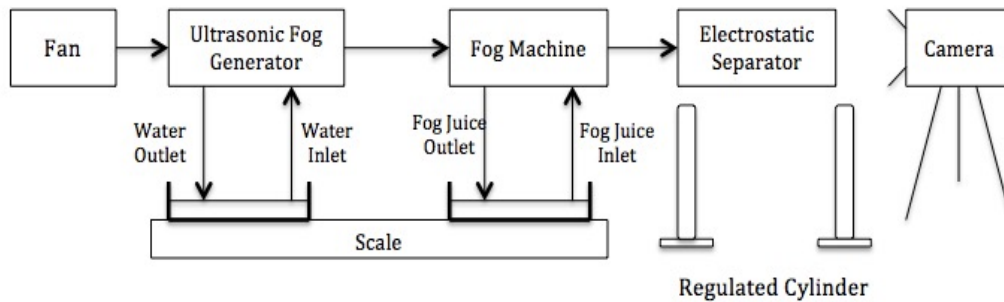
(b) Experiment setup sketch of wire-to-tube separator

Figure 16: Experiment setup for wire-to-tube electrostatic separator: (a) wire-to-tube separator experiment setup; (b) experiment setup sketch of wire-to-tube separator

A detailed view of the separator is shown in Figure 17. It is located at the end of the wire-to-tube separator system. In Figure 17, the diameter of the electrostatic separator is 1 inch. It is placed in the center of the outer tube. Blue rubber annulus is used to stand the tube and ensure that the air and particles will only go through the separator. Two regulated cylinders are placed at both upstream and downstream of the system. Since some particles accumulate before entering the

separator, a regulated cylinder is located at upstream to collect the accumulated liquid. The other one is used to collect separated liquid from electrostatic separator.

Spring   Drainage holes

(a) Cylindrical separator
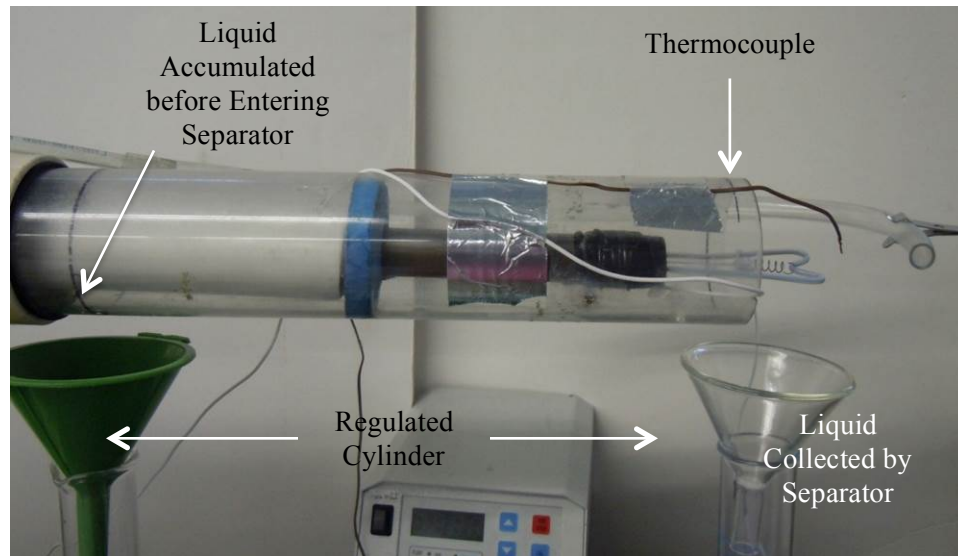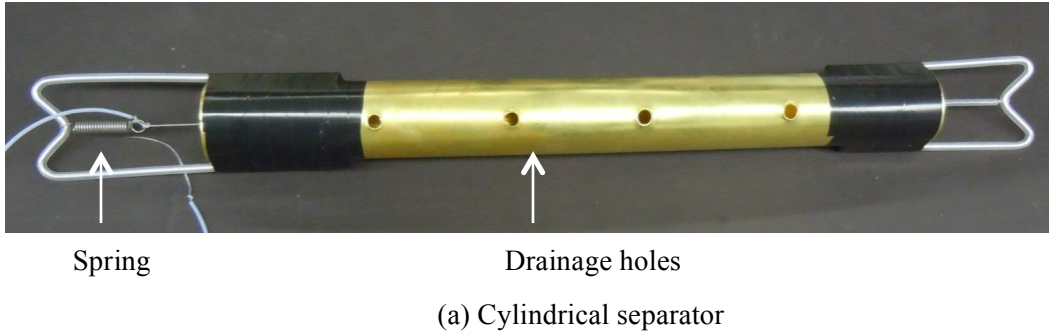
(b) Electrostatic separator system
Figure 17: Detailed view of electrostatic separator system: (a) cylindrical separator; (b) electrostatic separator system.

Efficiency is calculated by the ratio of the weight collected and injected into the system, shown by Equation 4.2. Injection rate of fog machine is assumed to be constant and measured. A scale is used to measure the net amount of water entering the system. Water and fog juice collected by the separator is collected by the regulated cylinder placed below the separator outlet. By measuring the dry bulb temperature and wet bulb temperature at both inlet and outlet of the system, the

humidity of the air is acquired through psychrometric chart of water. Therefore, the rate of particles vaporized in the system can be calculated.

$$Efficiency = \frac{Amount\ of\ liquid\ collected\ by\ regulated\ cylinder}{Net\ Injection\ Rate - Evaporation\ Rate} \qquad (12)$$

4.3.2 Experiments

Different tube-type electrode designs are studied to investigate and improve collection efficiency. Then, the influences of certain factors on separator performance are studied, including airflow velocity and different diameter of tube.

For different designs of electrodes, in order to meet the project constraints, certain parameters of the system are kept constant. The total length and diameter of the separator is constrained to 14 inches and 1 inch, respectively. The voltage connected to the separator is always 10.5kV. The concentration of particles is relatively constant, about 22 gram particles per one kilogram of airflow. Particle size is restricted to 1μm-5μm according to the requirements of test condition.

4.3.2.1 Multi-Stage Separator

It's observed that the plate type separator shows high collection efficiency due to the two-stage design. The concept of a multi-stage is implemented to the tube-type separator. Different designs of multi-stage separators are designed and tested, including two-stage separators and multi-stage separators.

The electrodes of two-stage separators are divided into a charging stage and a collection stage. The charging stage constitutes of thin wire. By supplying high voltage to the charging stage, the ionization process occurs and as particles pass through this stage they get charged. The collection stage is comprised of thick metal electrode. No ionization occurs at the collection stage. Although

36

in this stage the intensity of electric field between the charge and ground electrodes is lower, it is sufficient to deflect the charged droplets and have them collected.

Figure 18 shows different designs of the charged electrode. Design 1 is thin wire, used as reference group. Designs 2 and 3 are electrode designs of two-stage separators where the wire operates as the electrode for charging stage and the rod operates as the electrode for collection stage. In order to compare the influence of the diameter of the electrode for collection stage, different diameters of the rod for two-stage separator are tested, that is 3.2 mm and 6.4mm. Design 4 is the electrode of a multi-stage separator, which is segregated into four two-stage sections. A single stage design (Design 1) is also included into the group of experiments, which functions as a reference design.

(a) Actual electrode designs

Figure 18: Different multi-stage designs of electrode: electrode 1, thin wire, single stage electrode; electrode 2, two-stage electrode, second stage diameter 3.2mm; electrode 3, two-stage electrode, second stage diameter 6.4mm; electrode 4, multi-stage electrode

4.3.2.2 Different stage length experiments

Our study indicated that a two-stage separator shows higher collection efficiency. Further study is conducted to determine the appropriate proportion of the length of the charging stage and the collection stage. A long charging stage facilitates droplets charging while it may lead to insufficient length for the collection of droplets. On the other hand, a longer collection stage provides higher possibility that all droplets with different sizes are collected but that can be in expense of a deficiency in charging of droplets.

Four different electrode designs are tested as shown in Figure 19. The first electrode is a single-stage thin wire (Diameter 0.22mm; not shown in Figure 19 (a)). The other electrodes are all two-stage electrodes with a diameter of 6.4 mm for the second stage rod. The second electrode design has a longer charging length, 3/4 of total length. Third electrode design has an equal length of both the charging stage and the collection stage. The collection stage of the fourth design occupies 3/4 of the total length.

(a) Actual electrode designs
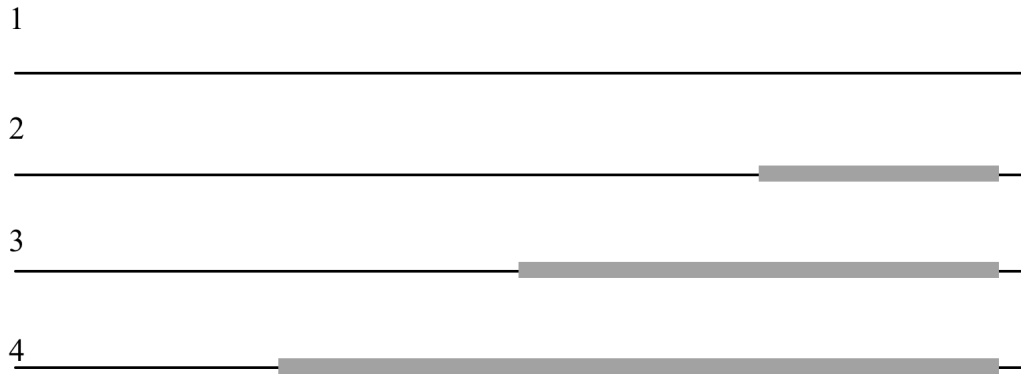
(b) Sketch of electrode designs

Figure 19: Different stage length designs of electrode: electrode 1, thin wire, single stage electrode; electrode 2, two-stage electrode, second stage length 1/4 of total length; electrode 3, two-stage electrode, second stage length 1/2 of total length; electrode 4, two-stage electrode, second stage length 3/4 of total length

4.3.2.3 Airflow Velocity Studies

The airflow velocity also has an important influence on the separator's collection efficiency. As the length of separator stays constant, the amount of time that the particles remain in the system (i.e. resident time) is proportional to the air velocity. Both the charging and the collection processes require some time to complete. If the resident time is excessively short, some particles might leave the system without reaching the tube wall, which results in low collection efficiency. If the resident time is too long, high efficiency can be achieved; but it may be just waste of separator space which is not desirable in real application. Hence, airflow velocity is regulated to obtain the highest airflow velocity, which still guarantees sufficient separation. A variable transformer regulates the velocity of airflow. Airflow velocity varies from 8m/s to 14m/s, measured by the anemometer at the outlet of separator. Collection efficiency was also measured for different airflow velocity as defined by Eq.13.

4.3.2.4 Diameter of Tube Studies

Different diameters of tube are studied experimentally. Three diameters of tube are investigated, including 1 inch, 1.5 inch and 2 inch. Figure 4.7 (a), (b), and (c) shows the upward view of the separators with their drainage holes. A sectional view of 2" diameter separator is shown in Figure 4.7 (d). Since based on the project requirements the physical envelope is constrained to a total diameter of 6.5 inches, by increasing the diameter of each tube, the number of tubes that can be fitted inside the envelope will reduce. That can be advantageous in terms of simplifying the fabrication process.

(a) Diameter of 1 Inch Separator
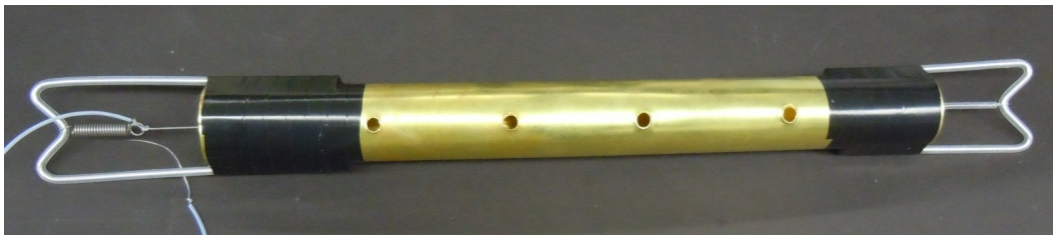
(b) Diameter of 1.5 inch Separator
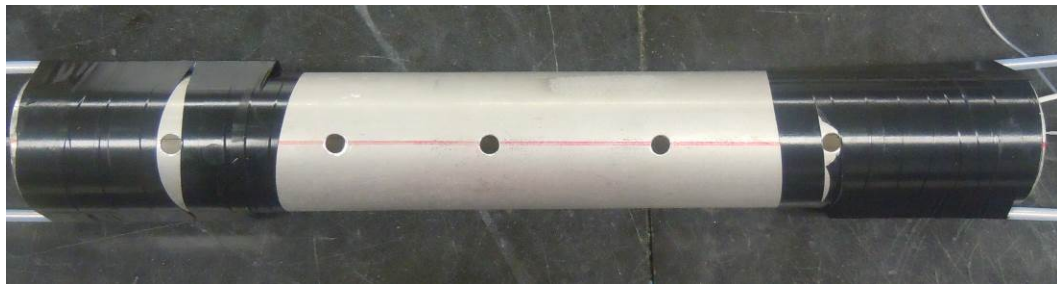
(b) Diameter of 2 Inch Separator
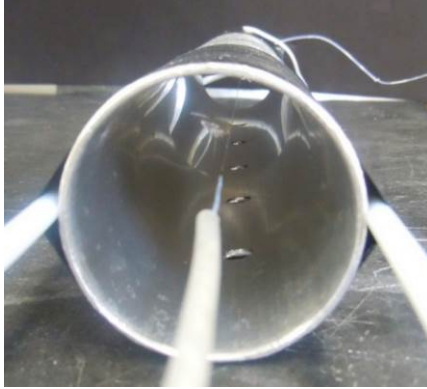
(c) *Lateral view of diameter of 2 inch separator*

Figure 20: Different diameter of tube separator: (a) diameter of 1 inch separator; (b) diameter of 1.5 inch separator; (c) diameter of 2 inch separator (d) Lateral view of diameter of 2 inch separator

In all experiments the air velocity is kept constant. This means the airflow rate for a larger diameter tube will be higher. Since the droplet generation rate of the ultrasonic fog generator cannot be regulated, the amount of water particles fed to the system is constant. In order to maintain a constant concentration for different separator designs, the fog machine is modified to regulate the fog concentration for different diameters of the tube separator. Figure 21shows the modified fog machine. A valve is installed at the inlet of fog machine to regulate the fog flow rate. Hence the concentration can be varied for different diameters of tube separator.
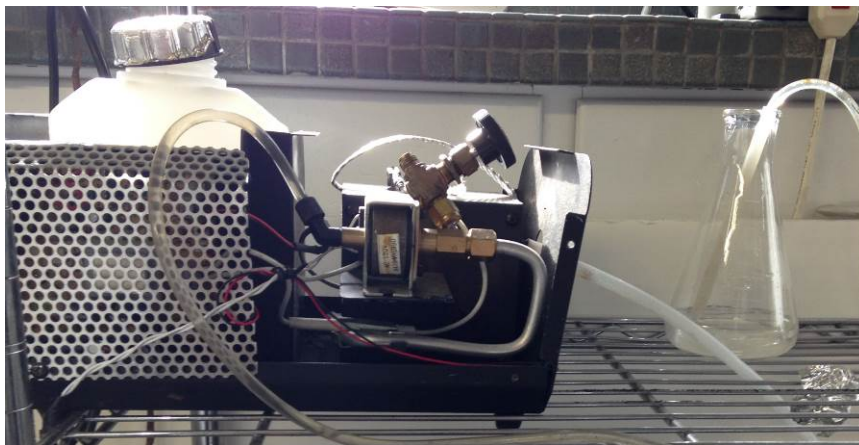
Figure 21: Modified fog machine

Different voltages are supplied to different sizes tubes to achieve the highest performance. However, voltage supplied to the system cannot exceed a certain value. When voltage exceeds the maximum voltage, sparking occurs. The sparks will influence the electric field and it is possible to cause a burning of the electrode, which will result in the separator failing to operate. Therefore, the highest voltage that the separator can operate safely will be supplied to the system to obtain the highest collection efficiency.

During the experiments, the V-I characteristics for different separator designs were measured. Moreover, to make the experiments comparable, both the concentration of particles and airflow velocity were also obtained for each experiment. Collection efficiency was calculated by measuring injection rate, and the amount of particles collected as shown by Eq.12.

4.4 Summary

In this chapter, the test setups for both wire-plate and wire-tube separators were introduced. In addition, different test conditions and electrode designs were discussed in detail. Then, a study on the influence of airflow and diameter of tube for wire-to-tube separator was described. Results and discussion of the experiments are presented in next chapter.

Chapter 5: Results and Discussion

5.1 Introduction

In this section the results of experiments, based on the test condition and methodology described in the chapter 4, will be discussed. First the wire-plate results are discussed to obtain the reasonable conclusion about the effect of using two-stage design versus single-stage design. Then, the results of the experiments for wire-tube are discussed. The results of the multi-stage separators are presented to determine which basic electrode designs will be selected and studied further. Next, the study on the effect of the stage length is discussed to determine the final design of the separator. Lastly, the results of the collection efficiency of the airflow effects and the diameter of the tubes specifically for two-stage designs are presented and reviewed.

5.2 Wire-to-Plate Separator Results

Current-voltage characteristics are measured for plate type separators as shown in Figure 5.1. These are separators 1 and 2 shown in Figure 14. Both separators show identical current voltage characteristics, which means the same electric characteristics for both separators. Since electric characteristics are an indication of the performance of separator, it can be concluded that both separators can operate similarly in separation processes.

Figure 22 demonstrates that the onset voltage for the plate type separator is about 5 kV. In order to get the separation process to occur, the voltage supplied to the separator should be higher than the onset voltage. To achieve the target efficiency, a certain voltage higher than the onset voltage must be supplied to the separator. However, a very high voltage would cause sparking in experiments. Therefore, the experiments are conducted by varying the voltage supplied to the charging stage to achieve required efficiency.

43
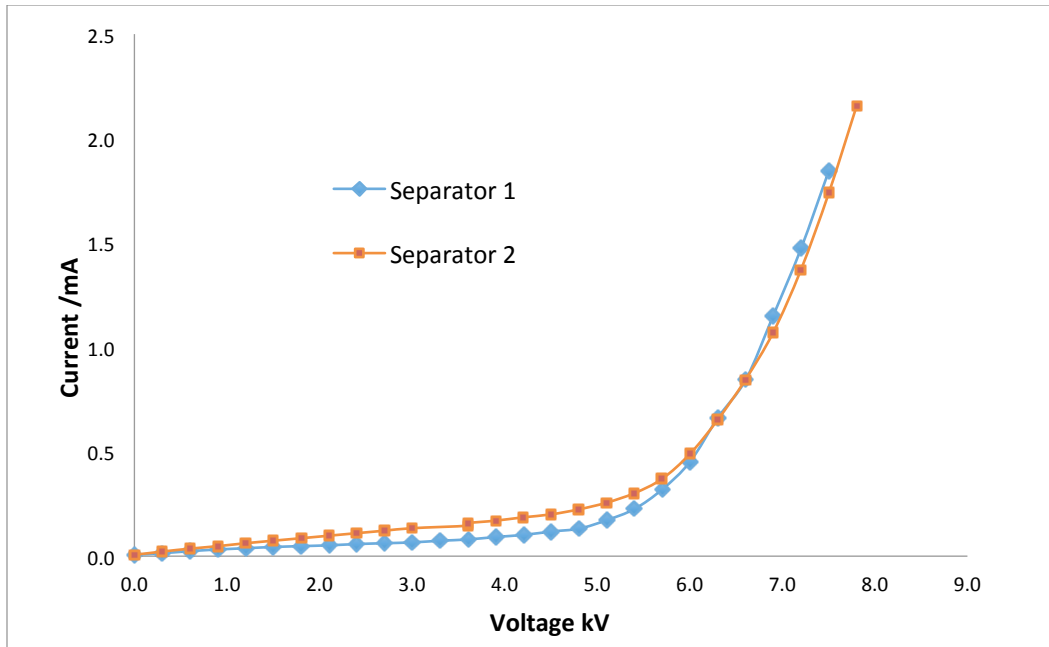
Figure 22: Current voltage characteristics

Figure 23 shows the experimental results for the plate type separator. The results are collected based on experiments described in section 4.2.2. It shows that the voltage supplied to the charging stage is positively affecting the performance of separator. By raising the supplied voltage, the measured opacity reduces which indicates the amount of fog collected by the separator increases and the collection efficiency improves.

As a reference case, the value of opacity for "no charge" is relatively constant, at about 95%. This value corresponds to the maximum amount of light blocked by droplets. When the voltage is equal to or lower than 5.1 kV (the onset voltage) the capability of collection for different separator conditions doesn't vary much. However, when the voltage is equal to or higher than 5.7kV, the difference between separator conditions becomes apparent.

Both two stage and one-stage separators can separate particles from flowing air. However, two-stage separators show higher collection efficiency than one stage. From Figure 23, compared to the other two experiment conditions, the "one stage" separator shows lower efficiency. Since

charging stage is not supplied with power, charged particles cannot be collected at charging stage, which leads to low separation performance.

As for the two-stage separator system, the "two-stage" shows better performance than "one charged wire". As mentioned in chapter 4, both "two-stage" and "one-charged wire" are two-stage separator systems. The only difference is that both the charging stages of separator 1 and 2 are supplied with the high voltage for "two-stage" separator while for "one-charged wire" only the charging stage of the first separator is supplied with high voltage. Therefore, the "two-stage" has a higher collection performance than "one-charged wire" due to secondary charging process.

From the experimental data, when charging stage separators are supplied with 7.5kV, the collection efficiencies are 96.3%, 71.9%, and 69.4% respectively for "two stage", "one charged wire", and "one stage". It must be noted that while the supplied voltage to charging stage are varied during these experiments, the voltage applied to collection stage are kept constant at 4.8 kV.
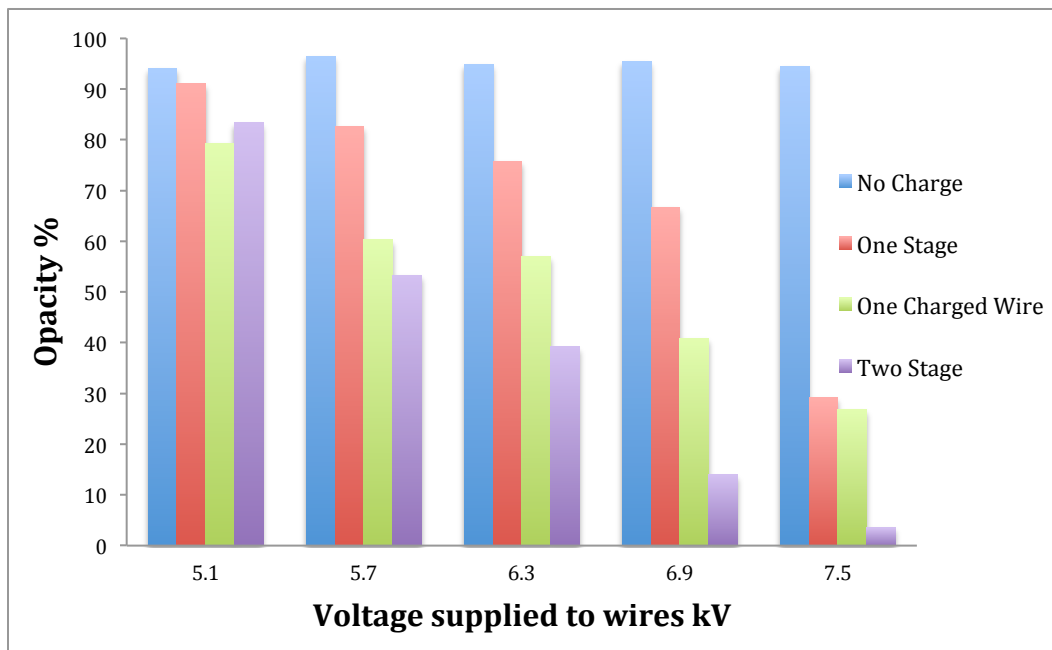
Figure 23: Results of different experiment conditions

45

Due to the difficulties in packaging the plate type separator in the required envelope, further

studies are conducted to investigate the possibilities of using tube type separators. The concept of

two-stage separator is further extended to the wire-tube separator to enhance the separator

efficiency.

5.3 Wire-to-Tube Separator Results

 5.3.1 Multi-stage Separator

Figure 24 shows the current voltage characteristics for different separator conditions, indicated in

Figure 18. As it can be seen, the onset voltages for all the electrode designs are about 6 kV.

Compared with the other electrode designs, single stage has a higher current when charged with

the same voltage. Current of both of the two-stage designs (shown in the figure as "Two stage

separator- 3.2 mm" and "Two stage separator- 6.4 mm") are identical, and the current value is

about half of the value for single stage. The Multi-stage separators have slightly higher currents

than the two-stage separators. Since the total length of the thin wire electrode is the same for

design 2, 3 and 4, the measured current is expected to be comparable for all of these designs. This

is due to the fact that only thin wire electrode participates in ionization process and creation of the

current. The results indicate that the power consumption of the system can be lowered by

changing the electrode design from single stage to two-stage.
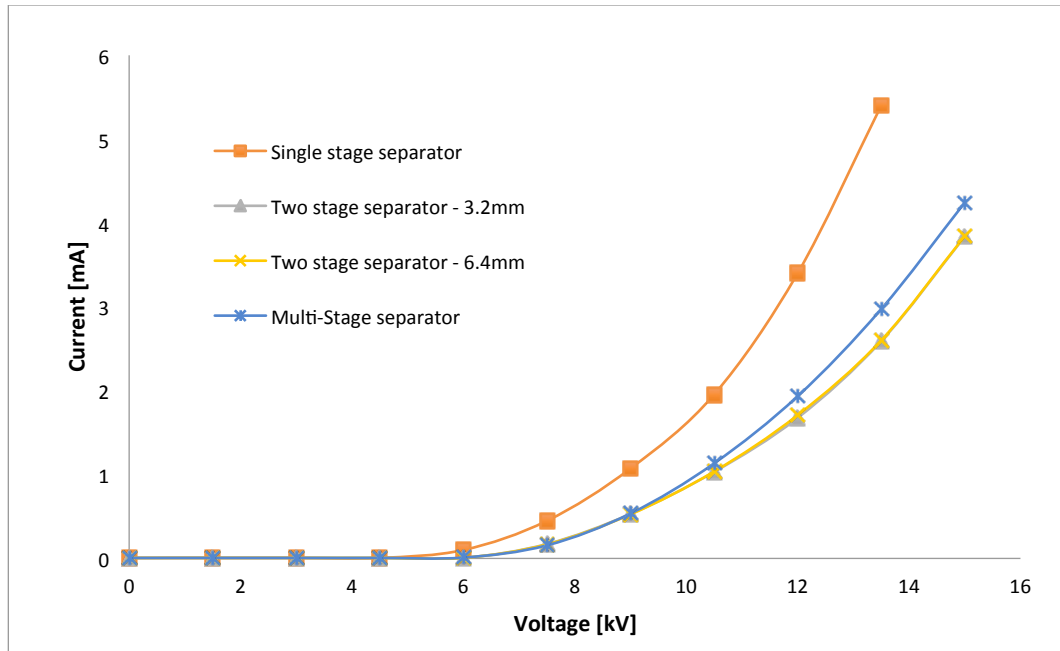
Figure 24: Current voltage characteristics for different separator conditions

Figure 25 illustrates the collection efficiency for different electrode designs when a constant voltage of 10.5 kV is supplying to separators. It is shown that both two-stage separators have collection efficiency over 90%. Collection efficiency of single stage and multi-stage design is slightly less than the two-stage design, about 70%.
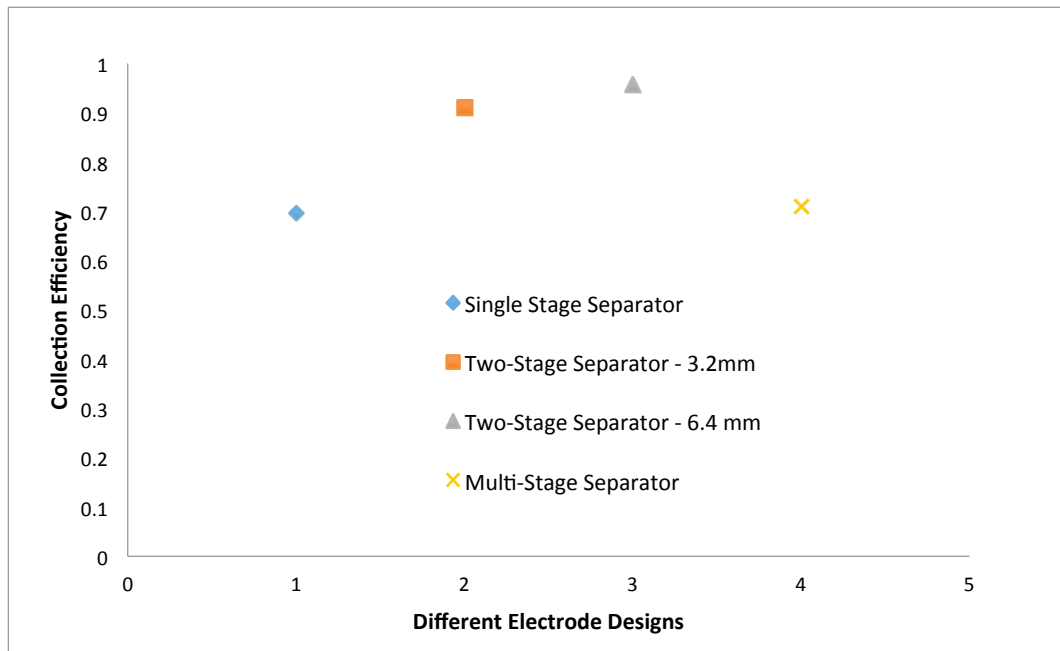
Figure 25: Collection efficiency for different separator conditions

It can be concluded from the collected data that two stage separators have higher collection efficiency than single stage and multi-stage separators. Both the charging and collection processes require certain amounts of time to allow for the processed at each stage to occur. For multi-stage separator, the electrode has been divided into four parts, so particles may not be charged and collected sufficiently due to the insufficient length of each part.

The diameter of the collection stage has barely any influence on the separator's performance. Since the diameter of the electrode at the collection stage does not cause the ionization effect, only collection processes occur. Due to the same electric fields for the different diameters of electrodes, the results show similar performance in the separators.

As two-stage separators have lower power consumption as well as higher performance, further studies about two-stage separators are conducted.

5.3.2 Study on the effect of stage length

According to the previous experiments, two-stage separators show higher performance than the single stage separators. Further studies to optimize the two-stage separators were performed.

Current voltage characteristics for different electrode designs (shown in Figure 19) are shown in Figure 26. For different electrode designs, onset voltage is almost the same, about 6kV. Single stage and 1/4 charging length have similar current voltage characteristics. With regard to a certain voltage, for example 12 kV, the current of the 3/4 charging stage separator is about a quarter of a single stage one, while the current of the 1/2 charging stage separator is about half of single stage separator. The results indicate that the power consumption of separator from low to high is shown in this sequence: 1/4 charging stage, 1/2 charging stage, 3/4 charging stage, and single stage. This seems reasonable because corona discharge occurs along the charging stage, and that is where the

current is induced. Hence, the charging length may directly influence the power consumption of the separator.
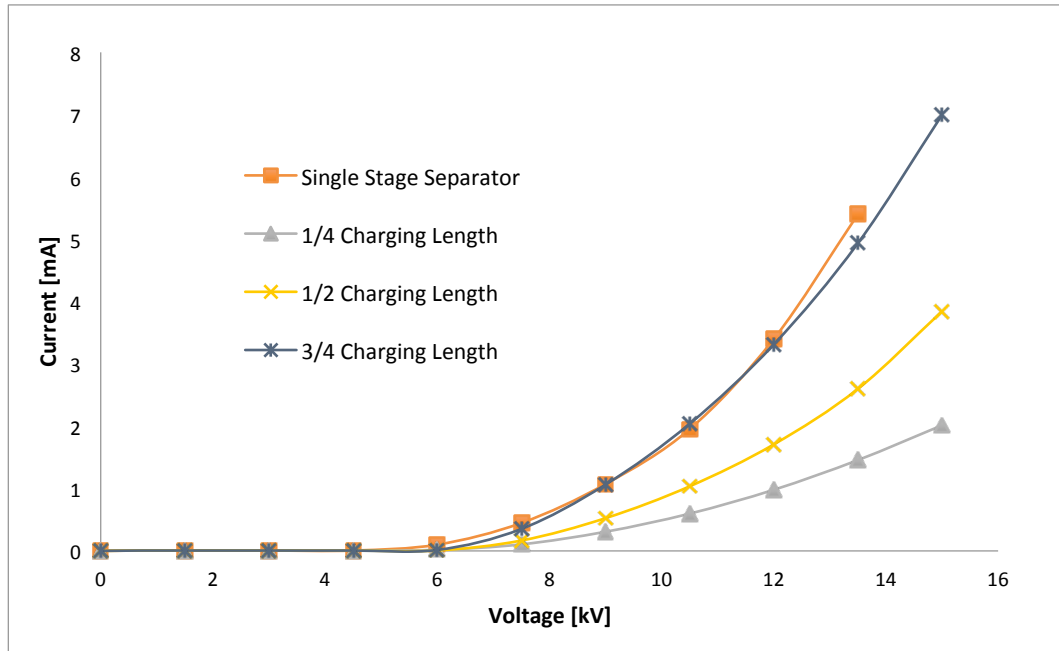
Figure 26: Current voltage characteristics for different separator conditions

In order to achieve high performance in the separators as well as lower power consumption in the systems, different charging stage length were studies. The collection efficiency of three designed electrodes is calculated from the experiments, shown in Figure 27. The single stage separator collection efficiency is presented as a baseline.

Figure 27 shows that 1/2 of the charging length stage has the highest collection efficiency, 93.8%, 1/4, and 3/4 charging length stages have similar collection efficiencies. Even though efficiency of these two designs is lower than the 1/2 charging length, it is still higher than the single stage separator. For 1/4 of the charging length separator, the charging stage only consists of 1/4 of the total length. Relatively low collection efficiency may result from the insufficient charging length. Some particles might leave the separator without being charged. Hence, the charging length should be long enough to charge all the particles. As for 3/4 charging length separators, it also

shows a comparably low performance. Particles can be charged sufficiently. However, due to

short collection length, some portion of particles may not have enough resident time to be

collected. Therefore, the 1/2 charging length separator shows highest performance.
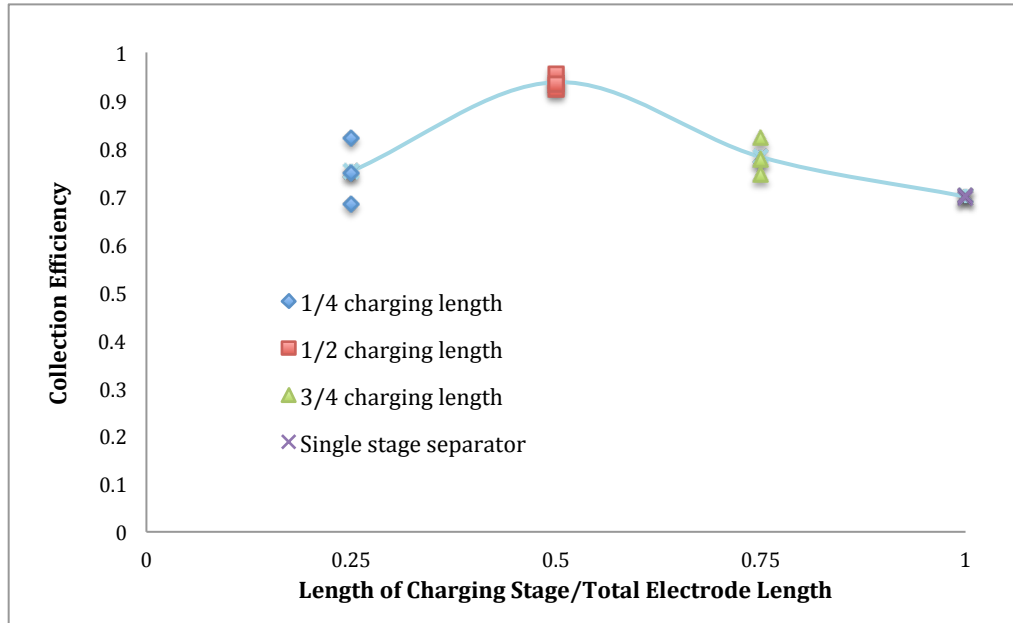
Figure 27: Collection efficiency for different separator conditions

5.3.3 Airflow Velocity Studies

From previous experiments, the final design is determined to be the two-stage separator with

equal charging and collection stage lengths. Further studies about the airflow were investigated.

Results of the influence of airflow velocity are shown in Figure 28.

When the velocity is equal to and lower than 10 m/s, the high efficiency of the separator can be

obtained. With increasing airflow velocity, the collection efficiency decreases gradually. The blue

line, shown in Figure 28, is the trend of decreasing collection efficiency with the airflow velocity.
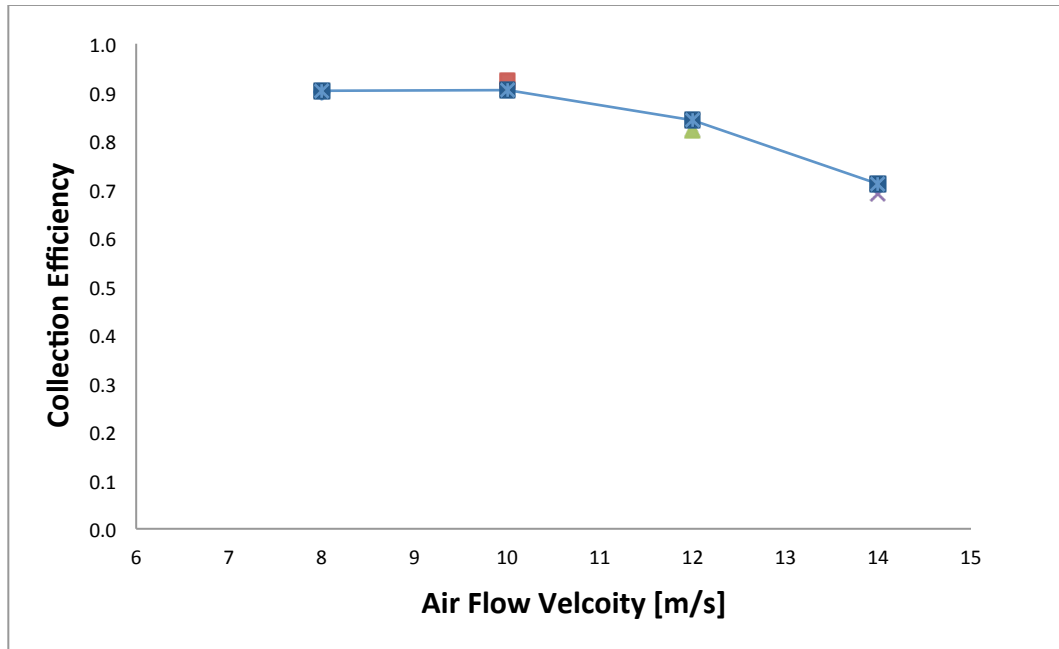
Figure 28: Collection efficiency at different flow velocity

Both charging and collection process requires a certain amount of time to complete. With the constant length of separator, increasing airflow velocity will lower the resident time of particles. From the experimental data, in order to ensure sufficient separation, velocity should be lower than at least 10 m/s.

5.3.4 Diameter of Tube Studies

Previous experiments were taken for single tubes with diameters of 1 inch. The influence of the different tube diameters is tested to study the characteristics of the electrostatic separator. From previous studies, the efficiency of 1 inch two-stage separator is roughly 93.8%.

Figure 29 shows that the performance of the separator with a diameter of 1.5 inches. Without power supplied, the performance of the separator is shown in Figure 29(a). By supplying a high voltage (21kV) to the system, most of the particles can be collected. Only a stream of fog can be observed from Figure 29(b).
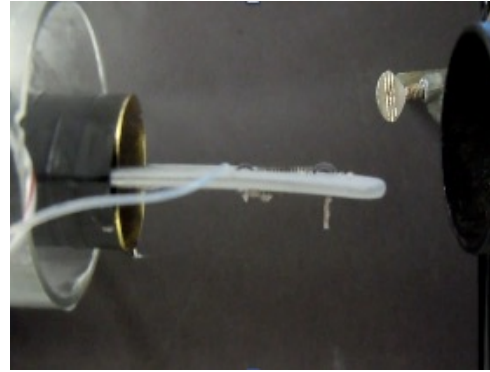
(a) Without Power	*(b) With Power*

Figure 29: Performance of diameter of 1.5 inch separator

For 2 inch diameter separators, two-stage separators were first tested at negative 24 kV. However, visualization study indicates that no obvious separation is observed. A possible reason for this is that the ionization processes does not provide enough electrons to charge all the particles. For uncharged particles, they will leave the separator directly. As for charged particles, due to the high concentration of particles, the path of the charged particles is blocked. Hence, the charged particles are not collected by tube wall.

5.4 Summary

In this chapter, the results of both the wire-plate separator and the wire-tube separator were discussed. The results of the wire-plate separator demonstrates that the two-stage separator design has a higher collection efficiency when compared to single-stage separator.

Then the idea of the two-stage electrode design was implemented in the wire-tube separator. Several experiments were conducted to improve collection efficiency for different electrode designs. It has been proven through the experiments that two-stage, ½ charging length wire-tube separators not only satisfy efficiency requirements, but also decreases the power consumption.

Then, the results of the influence of airflow velocity have been discussed. When the airflow velocity is lower than 10m/s, two-stage separators can achieve high collection efficiency. Lastly,

different diameters of tubes are studied. The study indicates that smaller diameters (1 inch and 1.5 inch) of tubes show better performance than the larger diameters (2 inch). The 1 inch separator demonstrates the highest collection efficiency among all the separators. Hence, the fabrication of the full scale prototype will utilize 1 inch, two-stage, and ½ charging length tube-type separators.

Chapter 6: Prototype Fabrication and Experiments

6.1 Introduction

In previous chapters study on a simple element of a full size separator, such as a single tube, was

presented. In order to meet the required capacity, it is needed that a full size electrostatic

separator prototype is built. This prototype incorporates several single element tubes operating in

parallel. In this section, a review of fabrication and experimental test of this prototype is

presented. First, the concept of area utilization is studied to identify the best design of the

prototype. Then, the prototype components are introduced. These components include face sheets,

electrode supports, separators, and electrodes. Specifically, for electrode support, stress and

displacement analysis results are presented. Then the experiments and test condition are described.

Finally, the study on the performance of the separator is also described.

6.2 Area Utilization Study

Area utilization is a very important factor in design of the prototype, since it influences the

airflow velocity. Area utilization (AU) is defined by equation 6.1.

$$AU = \frac{Number\ of\ Tube\ Separator \times Area\ of\ Each\ Separator}{Total\ Area\ of\ the\ Geometry} \qquad (14)$$

The area utilization indicates that from the total available physical envelop area what portion is

used as flow area. Since the available envelope is constrained to a diameter of 6.5 inches, for a

given total air flow rate, increasing area utilization will lead to lower air velocity. The air mass

flow rate is constant and the mass balance is given by equation 6.2. Since the density of the air is

constant as it goes through the separator, with increasing area utilization, the airflow velocity will

decrease. From studies in chapter 5, it was observed that high efficiency can be obtained at a

velocity of about 10 m/s or less. Hence, the study of area utilization can optimize the design of the prototype in order to achieve sufficient separation.

$$\dot{\mathbf{m}} = \rho \cdot \mathbf{V} \cdot A \qquad (15)$$
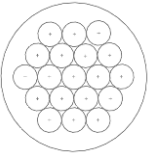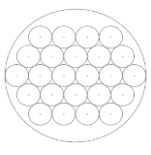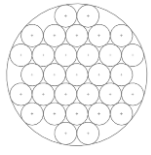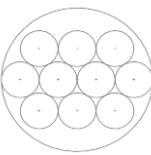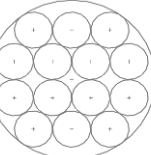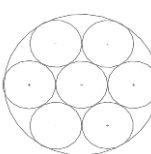
$$A = Area\ Utilization\ \cdot Total\ Area\ of\ the\ Geometry \qquad (16)$$

Bundle designs with different tube arrangements or diameters are shown in Table 4. With increasing number of tubes fitted in the bundle design, area utilization increases, which results in lower airflow velocity. The air velocity is calculated for a given total airflow rate of 0.189 kg/s (25 lb/min).

It was concluded from chapter 5 that the separator with a diameter of 1 inch and 1.5 inches works most effectively. Therefore, even though a 2 inch separator has a high area utilization and appropriate design, it can not be fabricated into the prototype, due to a poor performance for separation of high concentration droplets. As for 1.5 inch separators, the design with 10 tubes has a relatively low area utilization. Relatively, the velocity is higher, 11.3 m/s lading to insufficient separation. On the other hand, the design with 14 tubes does not function as well due the oversized bundle.

For 1 inch separators, the design of 19 separator tubes is abandoned due to the same reason of low area utilization. The other two designs appear to meet requirements of geometry constrains as well as low air velocity. Hence, the bundle sizes will be about 24 to 31 tubes. Taking geometry tolerance into consideration, further studies about the bundle design are discussed in the following chapter.

Table 4: Various bundle designs

Bundle Design	Separator Size	Bundle Size	Number of separators	Area Utilization	Air Velocity m/s
	1"	6"	19	52.8%	13.4
	1"	6"	24	66.7%	10.6
	1"	6.3"	31	78.1%	8.2
	1.5"	6"	10	62.5%	11.3
	1.5"	6.58"	14	71.9%	8.1
	2"	6"	7	77.8%	9. 1

6.3 Prototype Components

The prototype is composed of four main components, which are face sheets, electrode supports, separator tubes, and electrodes. Figure 30 shows the interior of the prototype design, which demonstrates the two-stage electrode design of the separator. The charging stage and the collection stage are marked in the figure. The airflow direction is also illustrated. Figure 31 is the full view of prototype, which includes a 24-tube bundle.
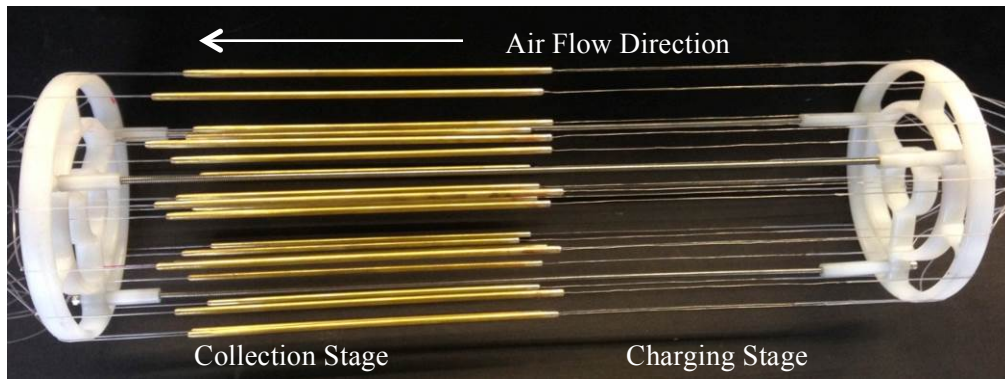
Figure 30: Interior of prototype design

Figure 31: Prototype full view

6.3.1 Face sheet

Figure 32 illustrates the face sheet. There are 24 circular holes where separator tubes are positioned. Since a distance of 2 mm between each hole is required to leave sufficient space to

hold each tube, provide a gap for water drainage and keep face sheet from deformation, the

diameter of the bundle size is increased to 6.5 inches.

The main purpose of the face sheet is to maintain the position of separator tubes. Two face sheets

are placed at both ends of the prototype. It is designed to make full use of the cross sectional area.

The bottom of the face sheet is cut to leave space for drainage.

The face sheet is made with brass. Since the face sheet is designed to hold the tubes tightly and it

is in direct contact with all tubes, when the face sheet is grounded, all the separator tubes will be

grounded accordingly.

Figure 32: Face sheet

6.3.2 Electrode Support

The main purpose of electrode support is to hold the electrodes sturdily in place. Figure 33 shows

the 3-D drawing of the electrode support. It was designed such that the electrodes will be located

precisely in the center of each separator tube and it can be fabricated in the onsite machine shop.

A detailed drawing of the places to hold the electrodes is illustrated in Figure 34. The electrode wire is imbedded in the grooves. A knot is placed in the hole to hold the electrode.
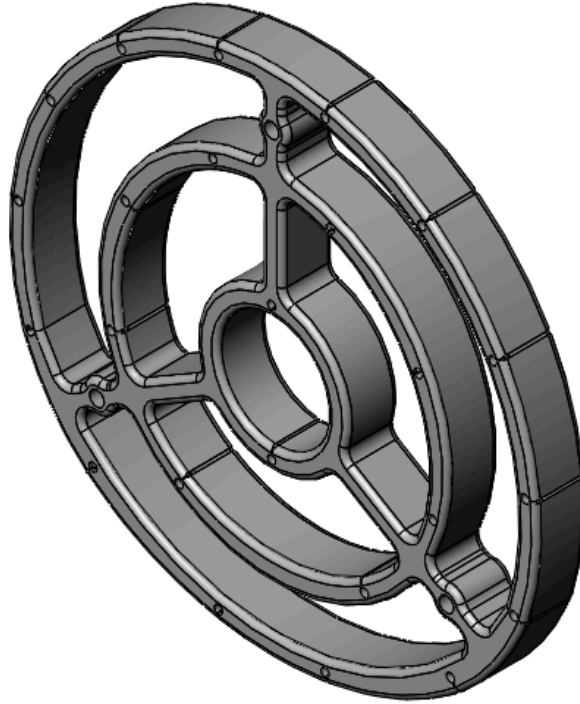
Figure 33: Electrode support
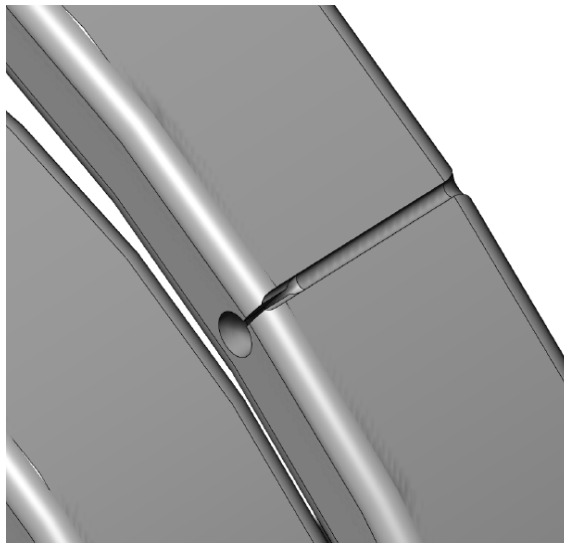
Figure 34: Detailed drawing of electrode support

Due to the force exerted on the electrode support from tension of each electrode, it is required to be designed to endure certain force (assumed 5N per electrode). Therefore, stress and displacement analysis were simulated with Solidwork software [solidworks].

SimulationXpress function was used to obtain the stress and displacement analysis. First, fixture locations are determined at the three holes, which are used to hold the electrode support. Second, the direction and value of exerting forces are added, shown as the red dots in the Figure 35. After the material is selected, we can run the simulation. Certain requirements should be met by the electrode support. Electrode support should be non-wettable. Also, the material needs to be electrically insulated. Different kinds of material were used in simulation to evaluate their structural performance. Accordingly PVDF was chosen to fabricate the electrode support. PVDF has the water absorption of 0.02%. The results of the simulation for PVDF are shown in Figure 35. Different colors represent the displacement of that location. Maximum displacement is 0.16mm, which is within the acceptable tolerance value.
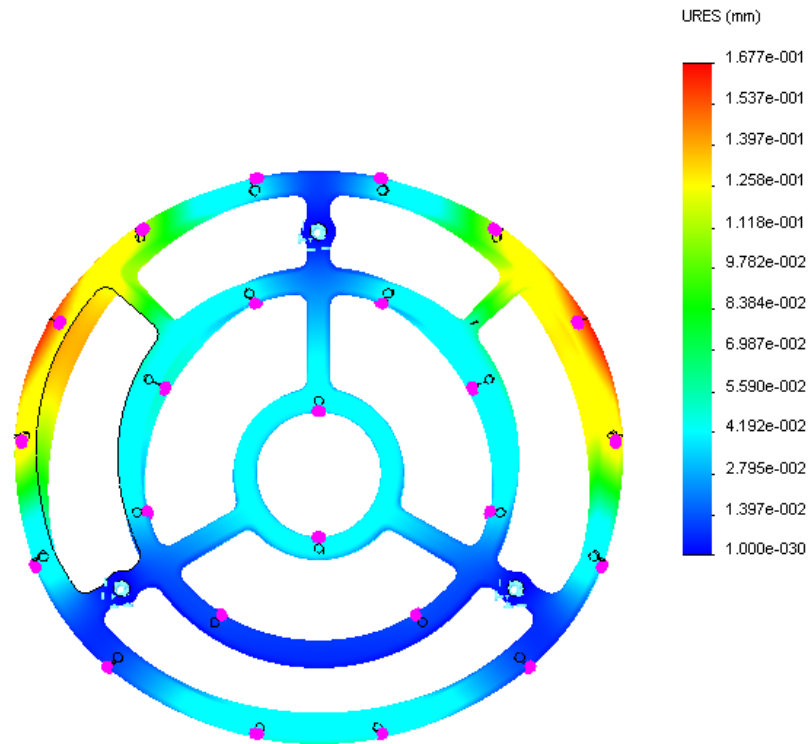
Figure 35: Result of simulation for PVDF

The electrode support fabricated is shown in Figure 36. The two electrode supports are fabricated identically from PVDF using mechanical machining. The edge of the separator is fabricated smoothly to guide the airflow.
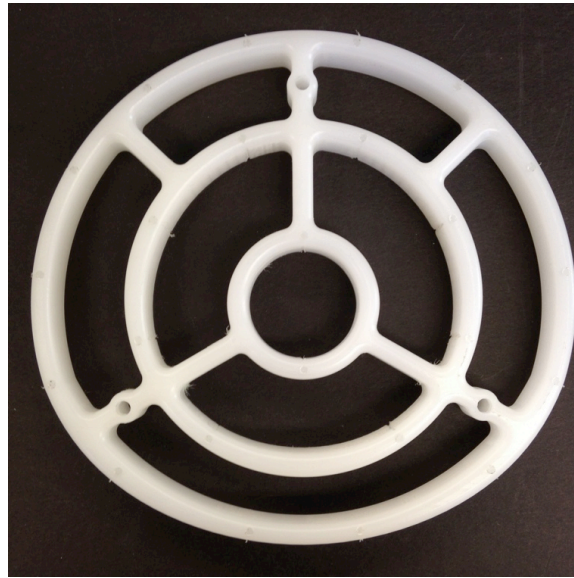
Figure 36: Electrode support

6.3.3 Separator Tubes

The separator tubes are made from brass. Three drainage holes were fabricated in line for each tube as shown in Figure 37. Since most of water collection process occurs downstream, it is important to locate the drainage holes near the outlet of separator. The holes were tapered such that they facilitated drainage of water.

Figure 37: Separator tube

6.3.4 Electrode

As the electrode is in two-stage design, it requires specific method to fabricate. Figure 38 and Figure 39 illustrate the configuration and dimensions of the electrode. The electrodes are composed of the charging stage and the collection stage. The charging stage is constituted of a thin wire. The corona effect occurs near the thin wire so particles can be charged. The collection stage is composed of a brass tube with a diameter of 3.2mm. The length of the charging stage is the same as the collection stage. At the ends of the electrode, knots were fabricated to hold the electrode on the electrode support.

Figure 38: Configuration of electrode
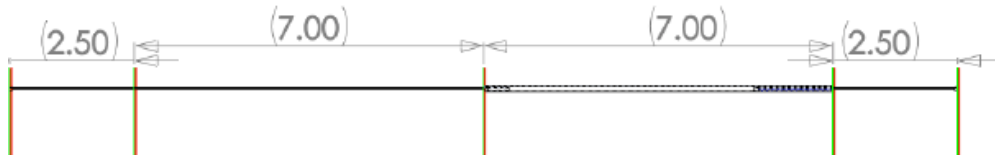
Figure 39: Dimensions of electrode

Figure 40 shows the inner configuration of the collection stage electrode. It is show that a spring is inserted inside of the collection stage tube to provide sufficient tension. Caps are also fabricated to seal the ends of collection electrodes as shown in Figure 41.

Figure 40: Inner configuration of collection stage
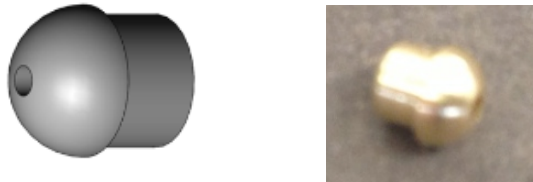
Figure 41: Cap design

6.4 Prototype Experiments

Figure 42 shows the experiment setup for the prototype bundle. Figure 42 (a) is an experimental setup for the test with the fog machine. Figure 42 (b) is used to test the particles produced by nozzle. The fan with the higher power is utilized to obtain higher velocity. The fog machine, shown in Figure 43, is used to generate micro-sized particles. However, as the capacity of fog machine is not sufficient for bundle separator, only part of the prototype is tested each time.
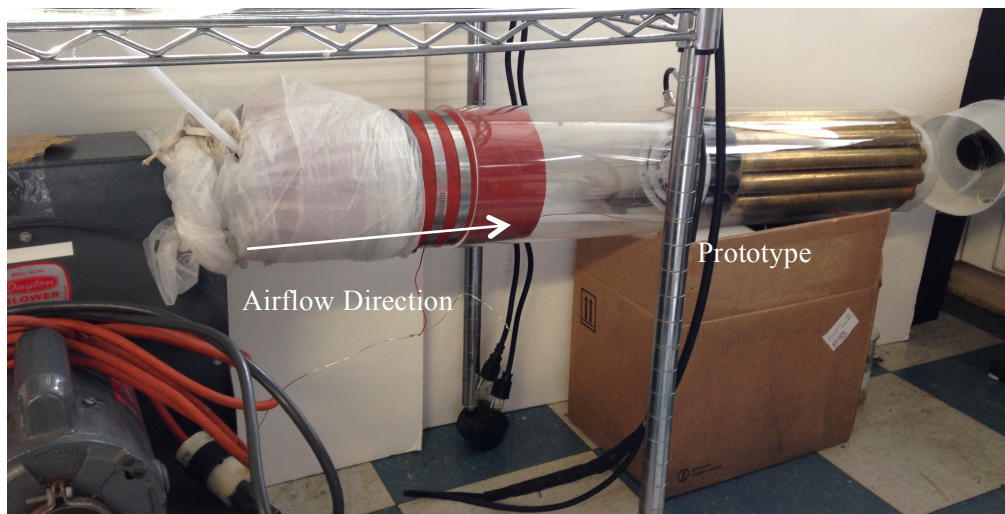
(a) Experiment setup for particles produced by fog machine
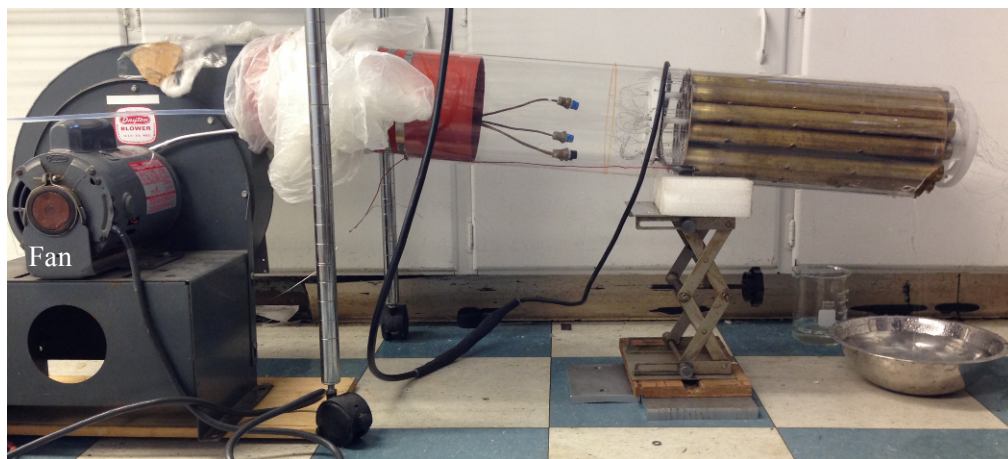
(b) Experiment setup for particles produced by nozzle

Figure 42: Experiment setup: (a) experiment setup for particles produced by fog machine; (b) experiment setup for particles produced by nozzle

The fan directs airflow into the mixing section upstream of the electrostatic separator. At the same, the fog juice particles are generated by either the fog machine or the nozzle, and then guided by a tube so they can flow into the channel. The separator prototype is connected to the mixing section of the channel. Droplets can be separated by the prototype as they flow through the tube bundle. They will be collected at the outlet of separator.
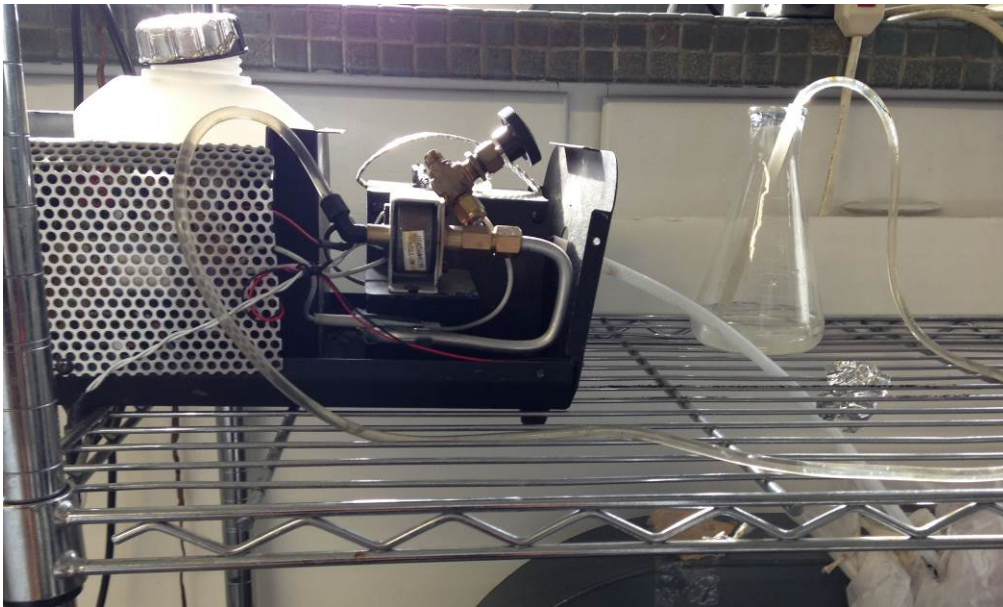
Figure 43: Fog generation system

6.4 Experiment Results and Discussion

As described before the capacity of the fog machine was not sufficient to test the performance of all the operating tubes at the same time. Therefore, different sections of the separator were tested, respectively. The performance of the separator is visually observed as shown in Figure 44.

When there is no power supplied to the separator, no separation process occurs. All the fog juice droplets pass through the system as shown in Figure 44 (a). When the separator is charged with a high voltage, the separation process occurs which collects all the droplets as shown in Figure 44 (b). This demonstrates the successful operation of the prototype.
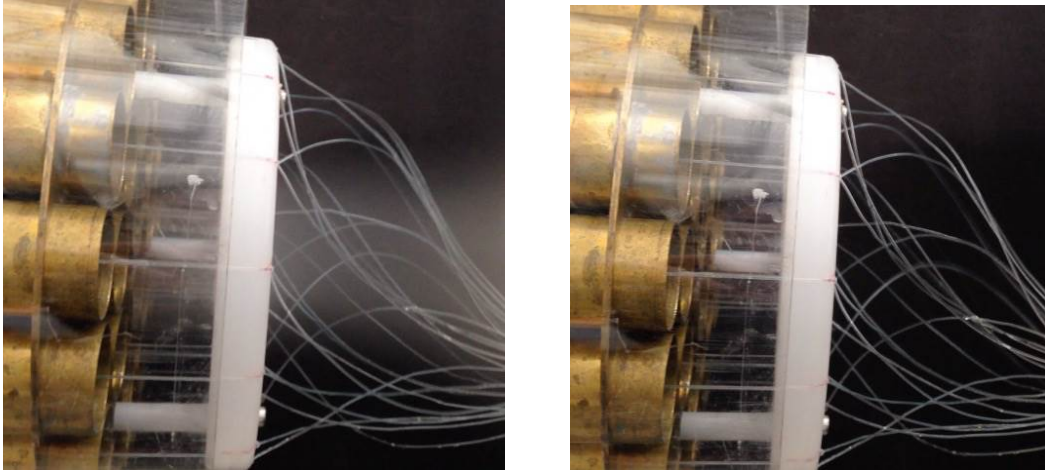
(a)   (b)

Figure 44: Performance of prototype

Experiments were also carried out for the particles produced by nozzle. This allowed us to

achieve the required concentration and operate all the separation tubes at the same time.

However, as discussed in section 2.2.3, the droplets size was way above the required test

condition (~100 μm and higher). During the experiments with droplets produced by nozzles,

sparking was observed. Figure 45 show that the sparks happened at the outlet of the prototype. It

was observed that the liquid accumulates at the bottom of each separator tube. This will directly

shorten the distance between the electrode and the grounded tube. The electric field between the

two exceeds the dielectric field strength of the air, which causes sparks. Two possible reasons

were proposed to explain this phenomenon. The first possible reason is the size of droplets. Since

the size of the droplets produced by nozzle is much larger than those produced by fog machine,

the particles can adhere to the electrode support easily, and then reenter the separator in the form

of large droplets. These large droplets accumulate at the inlet of separator tube, then causes

sparks. Another possible reason is the turbulence flow. Due to the sharp edge of separator inlet,

the air vortex might happen at the inlet of separator. The vortex then traps the particles to form

large droplets. This might also further lead to spark issues.

Figure 45: Spark issue in prototype

6.5 Summary

In this chapter, design fabrication and testing of a full size separator, which can meet the required test conditions, are described. Moreover, an overview of the concept of area utilization was presented. Different bundle designs specific to the various sizes of the separators were introduced. Then, the components of the prototype were described, including the face sheet, the electrode support, the separator tube, and the electrode. Particularly, in order to support the electrodes, stress and displacement analysis were simulated for the electrode support with SolidWorks. In addition, experiments were conducted to demonstrate the performance of the prototype. Two different droplet generation methods were utilized, which are the fog machine, and the nozzle. The prototype shows high performance when separating particles produced by the fog machine. However, sparks were observed with particles generated by nozzle. Possible reasons were proposed to better explain this issue.

Chapter 7: Conclusion and Further Work Recommendation

7.1 Conclusion

The current study indicated that both planar and cylindrical electrostatic separators have shown promising performance. However, the geometry constraints limit the overall geometry of the prototype to a circular shape, which makes the plate type separator difficult to package and fit in the given envelope. Hence, further numerical and experimental studies mainly were focused on the tube type separator.

Numerical simulations were first performed to understand the separation process and characteristics of the cylindrical separator. A computational code in Matlab environment was prepared to study the effects of both the electric field and the current density. It was concluded from the simulation results that a high electric field and current density occurs near the center of separator, in other words, near the charging wire. This phenomenon is called corona discharge. Particles, after entering the separator, can be ionized near the charging wire. For the current study, particles are charged with negative polarity. The grounded tube wall, which has relatively positive polarity, can collect negatively charged particles. Hence, the separation process completed.

Characteristics of particle migration in the separator were also numerically studied. Both the trajectory of the particles for different particle sizes and the collection efficiency at different supplied voltage were simulated with Engineering Equation Solver. The trajectory of the larger particles indicated higher collection efficiency with the same tube separator. Another simulation study demonstrated the relationship between collection efficiency and supplied voltage. It was noted that when supplied voltage was lower than the onset voltage, there was barely any separation of particles. However, with increasing the voltage supply, collection efficiency also increased gradually. After it reached a certain value, theoretically 100% efficiency was reached. It

indicates that the supplied voltage has a significant influence on the efficiency. Hence, for experimental studies, voltage supplied to the system should be at least higher than the onset voltage. Also, by increasing voltage, the maximum efficiency can be obtained.

Since two-stage planar separators showed higher performance than single stage, experimental studies mainly focused on the implementation of two-stage separators to cylindrical separators to further improve the collection efficiency. First, the three different designs of tube type separators were designed and fabricated, including two-stage and multi-stage separator. Experimental results show that the two-stage separator performed better than both the single stage and the multi-stage separator. Then another set of experiments was conducted to study the influence of various portions of the charging stage and collection stage on the performance of the separator. The results indicated that when the length of the charging stage and collection stage are the same, the separator demonstrated higher efficiency. Hence, for the full scale prototype design a two-stage separator with equal lengths for both the charging and collection stages is considered and implemented.

Also the characteristics of separator were experimentally studied, including the influence of the airflow velocity and the diameter of tube on separator efficiency. First, resident time is defined as the time it takes for a particle to travel through the separator. It is inversely proportional with the airflow velocity. With increasing velocity of air, particle resident time will decrease. The experiments indicated that lower airflow velocity showed higher separator performance, since particles had sufficient time to be charged and collected. Besides, the influence of the diameter of tube was also discussed. It was observed that, with similar test condition, a smaller separator with 1" diameter demonstrated higher performance when compared to the larger size of separator with 2" diameter.

A full-scale prototype was designed and fabricated with the two-stage electrode design with equal lengths in the charging and collection stages. The arrangement and the number of tubes were first designed. From the previous experimental study, it was shown that lowering airflow velocity could ensure higher separator performance. The concept of area utilization was used to improve the design of bundle. By increasing the area utilization, airflow velocity can be reduced. With various designs for different sizes of tube, the final design was selected based 1 inch tube diameter.

Most of the components of the prototype were first drawn in SolidWorks, then fabricated in the machine shop, including face sheets, electrodes, separator tubes, electrode supports, and outer tubes. The designs methodology of electrode supports and separator electrodes were discussed thoroughly in chapter 6. As discussed the material of the electrode support requires low water absorption and high rigidity. Different materials were simulated with SolidWorks. Based on structural simulation a final design created which uses PVDF as the material to fabricate the electrode support. As for the electrode, since some tension is required to keep them tightly fixed and in position, a tension mechanism consisting a set of springs needs to be designed. A final innovative design was adopted which was based on inserting springs into collection stage. This design required delicate work and significant effort to properly install the springs in their place.

Experiments were conducted to test the performance of the prototype. Due to the limitations of the laboratory experiments, the same test conditions with a single tube separator cannot be established. Therefore, the nozzle and the fog machine were utilized as an alternative. However, some test condition requirements cannot be met. Nozzles can provide sufficient concentration for the prototype, but the particles produced are in sizes over 100 microns, which is significantly higher than the requirements. While the fog machine can supply particles within the size requirements, the concentration is only enough to test a few tubes of separator at each test.

The experimental results of the prototype demonstrated the high performance of the unit for collecting particles produced by the fog machine. However, when atomized droplets supplied by the nozzle, the issue of spark occurred at both the inlet and the outlet of separator. As most sparks occurred at the inlet, few possible reasons were proposed to better explain the spark problem. It was observed that droplets accumulated at the inlet of separator. This could shorten the electrical distance between the electrode and the tube wall, which leads to sparking. The large particle sizes might cause the sparks due to a significant accumulation of droplets on the prototype components. Large droplets were observed on the electrode support, which were subsequently detached and then entered the separator with the airflow. This large lump of droplets can lead to accumulation of water at the tube entrance. Another possible reason is the influence of turbulence flow. The turbulence flow might create a vortex, which traps the liquid at the inlet of the separator.

7.2 Future Work Recommendation

In this study, the numerical method is used to understand certain characteristics of the electrostatic separator and particles qualitatively. As a recommendation for future work, other influencing factors on the electrostatic separator can be numerically simulated, for example, various diameters of the separator tubes, different electrode designs, and electrostatic separator designs. Moreover, the simulation can be extended to other design alternatives such as two-stage and multistage designs.

Another recommendation is to study the influence of different diameters on the separator's performance. For smaller particles (1~2μm), using smaller diameters for the tube separator shows higher efficiency than larger ones. However, the reason of this phenomenon is not fully understood. Further experimental studies can be conducted to determine the relationship between the size of droplets and optimum tube diameter. The characteristics of the particles such as particle size and its electrical characteristics can influence the separator efficiency. The numerical simulation of the tube type separator in this thesis demonstrates that larger particles can be

collected more easily than the smaller ones. However, corresponding experiments were not conducted to validate the results due to the laboratory test condition limitations. Besides, the influence of the particles' electric characteristics on the separator efficiency was not investigated in this thesis. Further studies can focus on the effect of characteristics of particles.

Another recommendation is to study the mechanism of spark issue. In this thesis, the sparks did not occur when the experiments were conducted on a single tube. However, it becomes an issue for the full-scale prototype. The primary disadvantage of the sparks is that it lowers collection efficiency of the separator. It may also burn the separator sensitive components since sparks can cause temperature to increase rapidly in the system. Hence, it is very important to better understand the spark issue and further solve the problem in the manufacturing application.

Appendix

Procedure DragCoefficient(Re:Cd)

if(Re<1e-7) Then Cd = 0.

If (1e-7<=Re) and (Re<0.4046) Then Cd = 24/Re

If (0.4046<=Re) and (Re<0.9023) Then Cd = 22.73/Re-0.0903/Re^2+3.69

If (0.9023<=Re) and (Re<9.996) Then Cd = 29.1667/Re-3.8889/Re^2+1.222

If (9.996<=Re) and (Re<100000) Then Cd = 46.5/Re-116.67/Re^2+0.6167

END

"Procedure: Determine whether the particle is collected or not"

Procedure CollectionCheck (Lpar, Rpar, Length, Rcylinder: collect$)

collect$:=' null'

if(Rpar=Rcylinder) and (Lpar< Length) Then collect$:=' Yes'

if (Length< Lpar) Then collect$:=' No'

END

"Boundary Conditions"

Rwire=0.022/2*10^(-2);

Dwire=2*Rwire*100;

Rcylinder=2.54/2*10^(-2);

Vwire=8400;

Vcylinder=0;

"Initial Location of Particle"

{ri=0.0002}

"ri=0.0005 to 0.0080, step is 0.0005"

"Parameters"

"Droplet size is changed from 3 micons to 10 microns"

Dp=3*10^(-6);   {Droplets size [m]}

RP=80;   {Relative permittivity of a particle, use water at 20 C}

Ke=9.0*10^9;   {Ke: Proportionality constant 9.0*10^9 [N*m^2/C^2]}

RhoA=1.1839;   {Density of air [kg/m^3] at 25 C}

RhoP=1000;   {Density of droplets [kg/m^3]}

Vis=1.983*10^(-5);   {Dynamic Fluid Viscosity [N*s/m^2=kg/ms] at 25 C}

U=10;   {Fluid velocity m/s}

g=9.8;   {acceleration due gravity [m/s2]}

per=8.85418781762*10^(-12);   {Permittivity}

IM=1.5*10^(-4);   {Ion Mobility}

"Relative Density [Unit: T: K, P: mmHg]"

T0=298;

P0=760;

T=298;

P=760;

RD=T0/T*P/P0;

"Current Density"

{Current=0.8*10^(-3);}

Current=0.966E-3   "Current is scaled to match the longer wire"

Length=35.5*10^(-2);

J=Current/Length

"Values of C1 and C2 are calculated from Matlab code"

a=(J/(2*3.14159*per*IM)*Rwire^2+C1)

b=(J/(2*3.14159*per*IM)*Rcylinder^2+C1)

Vwire=-(a)^.5+C1^.5*ln((a^.5+(C1)^.5)/Rwire)+C2

Vcylinder=-(b)^.5+C1^.5*ln(((b)^.5+(C1)^.5)/Rcylinder)+C2

{Emax=E0}

"C1 = 1279396.02804183761373464487905209"

"C2 = -10414.8906345229852249252251657637"

"Threshold Field Strength"

Emax=(30*RD+9*(2*RD/Dwire)^0.5)*10^5   "Upper limit"

{Emax=(Vwire-Vcylinder)/(Rcylinder-Rwire)}   "Lower limit"

"Electric Field"

E=(J/(2*pi*per*IM)+C1/r^2)^.5

E0=(J/(2*pi*per*IM)+C1/Rwire^2)^.5

"Ionic Charge Density"

RhoI=J/(2*pi*r*E*IM)   {RhoI=J/(E*IM)}

"Field Charging"

{Qfld=3*RP/(RP+2)*E*Dp^2/(4*Ke)}

Qfld=(3*RP/(RP+2))*(E*Dp^2/(4*Ke))*(3.14159*Ke*IM*RhoI*time/(1+3.14159*Ke*IM*RhoI
*time))

"Electrostatic body force exerted on a charged aerosol"

Fe=Qfld*E/(1/6*pi*Dp^3*RhoP)

"Equations used to calculate Up, Re, and Cd"

Fd=Cd*Re/24*18*vis/(RhoP*Dp^2)

dupdt=Fd*(-Up)+Fe

Re=RhoA*Dp*abs(Up-U)/vis

Call DragCoefficient(Re:Cd)   "It is used to calaculate parametric table 1"

{Cd=24/Re }   "It is used to calaculate parametric table 2 and 3"

"Time"

TimeR=Length/U*1.5   "Time is expanded"

{TimeC=Rcylinder/Up}

Constant=(1/6*pi*Dp^3*RhoP)*Cd*Re/24*18*vis/(RhoP*Dp^2)*(RP+2)*(4*Ke)/(3*RP*Dp^2)

"Collection Length"

Up=integral(dupdt,time,0,TimeR)

r=integral(Up,time,0,TimeR)+ri

Rpar=min(r,Rcylinder)

Vp=U*((1-Rpar/Rcylinder))^(1/7)

Lpar=integral(Vp,time,0,TimeR)

Call CollectionCheck (Lpar, Rpar, Length, Rcylinder: collect$)

Ratio=(1-(ri^2-Rwire^2)/(Rcylinder^2-Rwire^2))*100

V_onset=Rwire*Emax*ln(Rcylinder/Rwire)

$IntegralTable time:0.00005, Up, Cd, r,Lpar, Rpar,Qfld, collect$

By running program from appendix A, results are shown in Figure 46.
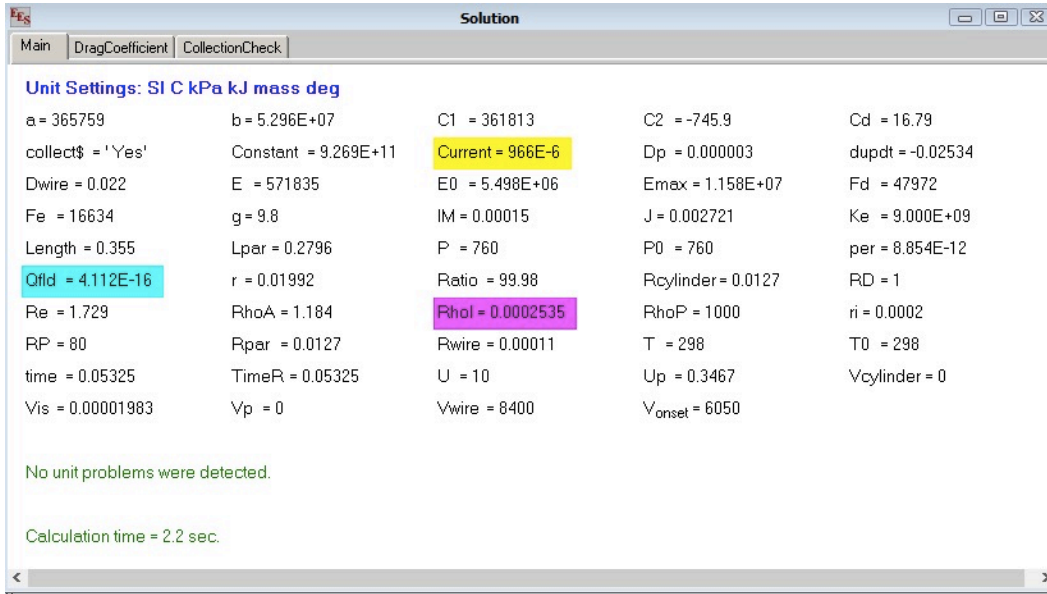
(a) Main result

(b) Drag coefficient

(c)
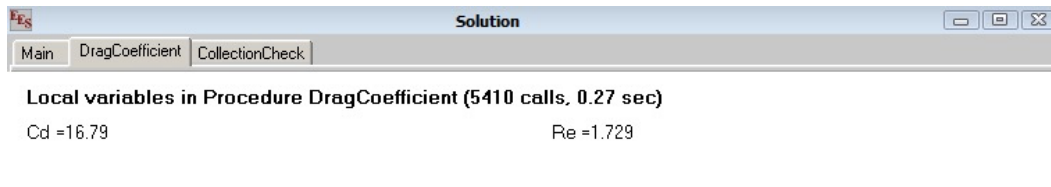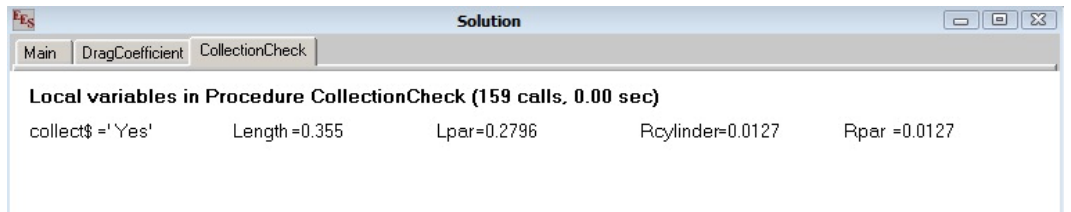
Collection check

Figure 46: Results of EES code: (a) main results; (b) drag coefficient; (c) collection check

From the results, it can be concluded that particles with size of 3 micron can be collected at 27.96 cm from the entrance of separator.

time	Up	Cd	r	Lpar	Rpar	Qfld	collect$
0	0	16.29	0.0002	0	0.0002	0	null
0.00005	1.84	19.54	0.0002653	0.0004986	0.0002653	7.624E-16	null
0.0001	2.899	21.8	0.0003725	0.000997	0.0003725	8.243E-16	null
0.00015	1.821	19.38	0.0004889	0.001495	0.0004889	7.309E-16	null
0.0002	1.416	18.59	0.0005652	0.001991	0.0005652	6.915E-16	null
0.00025	1.219	18.22	0.0006272	0.002488	0.0006272	6.648E-16	null
0.0003	1.041	17.89	0.000687	0.002984	0.000687	6.398E-16	null
0.00035	0.9723	17.77	0.0007338	0.00348	0.0007338	6.246E-16	null
0.0004	0.9035	17.66	0.0007806	0.003976	0.0007806	6.094E-16	null
0.00045	0.8346	17.55	0.0008274	0.004471	0.0008274	5.941E-16	null
0.0005	0.8003	17.49	0.0008663	0.004966	0.0008663	5.843E-16	null
0.00055	0.766	17.44	0.0009051	0.005461	0.0009051	5.744E-16	null
0.0006	0.7317	17.38	0.000944	0.005955	0.000944	5.645E-16	null
0.00065	0.7082	17.34	0.0009785	0.00645	0.0009785	5.573E-16	null
0.0007	0.6847	17.31	0.001013	0.006944	0.001013	5.501E-16	null
0.00075	0.6612	17.27	0.001048	0.007438	0.001048	5.430E-16	null
0.0008	0.6485	17.25	0.001078	0.007931	0.001078	5.384E-16	null
0.00085	0.6358	17.23	0.001108	0.008424	0.001108	5.339E-16	null
0.0009	0.6231	17.21	0.001138	0.008917	0.001138	5.293E-16	null
0.00095	0.6104	17.19	0.001168	0.00941	0.001168	5.248E-16	null
0.001	0.5977	17.17	0.001198	0.009903	0.001198	5.202E-16	null
0.00105	0.585	17.15	0.001228	0.0104	0.001228	5.157E-16	null
0.0011	0.5723	17.13	0.001258	0.01089	0.001258	5.111E-16	null
0.00115	0.5596	17.11	0.001288	0.01138	0.001288	5.066E-16	null
0.0012	0.5469	17.09	0.001319	0.01188	0.001319	5.020E-16	null
0.00125	0.5406	17.08	0.001345	0.01237	0.001345	4.995E-16	null
0.0013	0.5342	17.07	0.001371	0.01286	0.001371	4.970E-16	null
0.00135	0.5278	17.06	0.001397	0.01335	0.001397	4.944E-16	null
0.0014	0.5215	17.05	0.001423	0.01384	0.001423	4.919E-16	null
0.00145	0.5151	17.04	0.001449	0.01433	0.001449	4.894E-16	null
0.0015	0.5087	17.03	0.001475	0.01482	0.001475	4.868E-16	null
0.00155	0.5024	17.02	0.001501	0.01532	0.001501	4.843E-16	null
0.0016	0.496	17.01	0.001527	0.01581	0.001527	4.818E-16	null
0.00165	0.4922	17.01	0.001551	0.0163	0.001551	4.801E-16	null

is an example of parametric study results particle with size of 3 micron. In last column, null indicates particle at that location cannot be collected. The first "yes" means that particle with that initial location can be collected. Some data were omitted due to limited space.

Table 5: Results of particles of 3 micro

time	Up	Cd	r	Lpar	Rpar	Qfld	collect$

0	0	16.29	0.0002	0	0.0002	0	null
0.00005	1.84	19.54	0.0002653	0.0004986	0.0002653	7.624E-16	null
0.0001	2.899	21.8	0.0003725	0.000997	0.0003725	8.243E-16	null
0.00015	1.821	19.38	0.0004889	0.001495	0.0004889	7.309E-16	null
0.0002	1.416	18.59	0.0005652	0.001991	0.0005652	6.915E-16	null
0.00025	1.219	18.22	0.0006272	0.002488	0.0006272	6.648E-16	null
0.0003	1.041	17.89	0.000687	0.002984	0.000687	6.398E-16	null
0.00035	0.9723	17.77	0.0007338	0.00348	0.0007338	6.246E-16	null
0.0004	0.9035	17.66	0.0007806	0.003976	0.0007806	6.094E-16	null
0.00045	0.8346	17.55	0.0008274	0.004471	0.0008274	5.941E-16	null
0.0005	0.8003	17.49	0.0008663	0.004966	0.0008663	5.843E-16	null
0.00055	0.766	17.44	0.0009051	0.005461	0.0009051	5.744E-16	null
0.0006	0.7317	17.38	0.000944	0.005955	0.000944	5.645E-16	null
0.00065	0.7082	17.34	0.0009785	0.00645	0.0009785	5.573E-16	null
0.0007	0.6847	17.31	0.001013	0.006944	0.001013	5.501E-16	null
0.00075	0.6612	17.27	0.001048	0.007438	0.001048	5.430E-16	null
0.0008	0.6485	17.25	0.001078	0.007931	0.001078	5.384E-16	null
0.00085	0.6358	17.23	0.001108	0.008424	0.001108	5.339E-16	null
0.0009	0.6231	17.21	0.001138	0.008917	0.001138	5.293E-16	null
0.00095	0.6104	17.19	0.001168	0.00941	0.001168	5.248E-16	null
0.001	0.5977	17.17	0.001198	0.009903	0.001198	5.202E-16	null
0.00105	0.585	17.15	0.001228	0.0104	0.001228	5.157E-16	null
0.0011	0.5723	17.13	0.001258	0.01089	0.001258	5.111E-16	null
0.00115	0.5596	17.11	0.001288	0.01138	0.001288	5.066E-16	null
0.0012	0.5469	17.09	0.001319	0.01188	0.001319	5.020E-16	null
0.00125	0.5406	17.08	0.001345	0.01237	0.001345	4.995E-16	null
0.0013	0.5342	17.07	0.001371	0.01286	0.001371	4.970E-16	null
0.00135	0.5278	17.06	0.001397	0.01335	0.001397	4.944E-16	null
0.0014	0.5215	17.05	0.001423	0.01384	0.001423	4.919E-16	null
0.00145	0.5151	17.04	0.001449	0.01433	0.001449	4.894E-16	null
0.0015	0.5087	17.03	0.001475	0.01482	0.001475	4.868E-16	null
0.00155	0.5024	17.02	0.001501	0.01532	0.001501	4.843E-16	null
0.0016	0.496	17.01	0.001527	0.01581	0.001527	4.818E-16	null
0.00165	0.4922	17.01	0.001551	0.0163	0.001551	4.801E-16	null

0.0017	0.4883	17	0.001575	0.01679	0.001575	4.784E-16	null
0.00175	0.4845	17	0.001599	0.01728	0.001599	4.767E-16	null
0.0018	0.4806	16.99	0.001623	0.01777	0.001623	4.750E-16	null
0.00185	0.4768	16.99	0.001647	0.01826	0.001647	4.733E-16	null
0.0019	0.4729	16.98	0.001671	0.01875	0.001671	4.716E-16	null
0.00195	0.4691	16.97	0.001695	0.01924	0.001695	4.699E-16	null
0.002	0.4652	16.97	0.001719	0.01973	0.001719	4.683E-16	null
0.00205	0.463	16.96	0.001741	0.02022	0.001741	4.673E-16	null
0.0021	0.4608	16.96	0.001763	0.02071	0.001763	4.663E-16	null
0.00215	0.4587	16.96	0.001785	0.02119	0.001785	4.653E-16	null
0.0022	0.4565	16.95	0.001807	0.02168	0.001807	4.643E-16	null
0.00225	0.4543	16.95	0.001829	0.02217	0.001829	4.633E-16	null
0.0023	0.4521	16.95	0.001851	0.02266	0.001851	4.623E-16	null
0.00235	0.4499	16.94	0.001873	0.02315	0.001873	4.613E-16	null
0.0024	0.4477	16.94	0.001895	0.02364	0.001895	4.604E-16	null
0.00245	0.4456	16.94	0.001917	0.02412	0.001917	4.594E-16	null
0.0025	0.4434	16.93	0.001939	0.02461	0.001939	4.584E-16	null
0.00255	0.4412	16.93	0.001962	0.0251	0.001962	4.574E-16	null
0.0026	0.439	16.93	0.001984	0.02559	0.001984	4.564E-16	null
0.00265	0.4368	16.92	0.002006	0.02608	0.002006	4.554E-16	null
0.0027	0.4346	16.92	0.002028	0.02657	0.002028	4.544E-16	null
0.00275	0.4325	16.92	0.00205	0.02706	0.00205	4.535E-16	null
0.0028	0.4303	16.91	0.002072	0.02754	0.002072	4.525E-16	null
0.00285	0.4281	16.91	0.002094	0.02803	0.002094	4.515E-16	null
0.0029	0.4259	16.91	0.002116	0.02852	0.002116	4.505E-16	null
0.00295	0.4237	16.91	0.002138	0.02901	0.002138	4.495E-16	null
. . . . .							
0.03185	0.348	16.79	0.01249	0.2767	0.01249	4.118E-16	null
0.0319	0.3479	16.79	0.01251	0.277	0.01251	4.118E-16	null
0.03195	0.3479	16.79	0.01253	0.2772	0.01253	4.118E-16	null
0.032	0.3479	16.79	0.01254	0.2775	0.01254	4.118E-16	null
0.03205	0.3479	16.79	0.01256	0.2778	0.01256	4.117E-16	null
0.0321	0.3479	16.79	0.01258	0.2781	0.01258	4.117E-16	null
0.03215	0.3479	16.79	0.01259	0.2783	0.01259	4.117E-16	null
0.0322	0.3479	16.79	0.01261	0.2786	0.01261	4.117E-16	null
0.03225	0.3479	16.79	0.01263	0.2788	0.01263	4.117E-16	null
0.0323	0.3479	16.79	0.01265	0.279	0.01265	4.117E-16	null
0.03235	0.3479	16.79	0.01266	0.2793	0.01266	4.117E-16	null
0.0324	0.3479	16.79	0.01268	0.2795	0.01268	4.117E-16	null
0.03245	0.3479	16.79	0.0127	0.2796	0.0127	4.117E-16	Yes
0.0325	0.3479	16.79	0.01272	0.2796	0.0127	4.117E-16	Yes
0.03255	0.3479	16.79	0.01273	0.2796	0.0127	4.117E-16	Yes
0.0326	0.3479	16.79	0.01275	0.2796	0.0127	4.117E-16	Yes
0.03265	0.3478	16.79	0.01277	0.2796	0.0127	4.117E-16	Yes
0.0327	0.3478	16.79	0.01279	0.2796	0.0127	4.117E-16	Yes
0.03275	0.3478	16.79	0.0128	0.2796	0.0127	4.117E-16	Yes
0.0328	0.3478	16.79	0.01282	0.2796	0.0127	4.117E-16	Yes
0.03285	0.3478	16.79	0.01284	0.2796	0.0127	4.117E-16	Yes
0.0329	0.3478	16.79	0.01286	0.2796	0.0127	4.117E-16	Yes
0.03295	0.3478	16.79	0.01287	0.2796	0.0127	4.117E-16	Yes
0.033	0.3478	16.79	0.01289	0.2796	0.0127	4.117E-16	Yes
0.03305	0.3478	16.79	0.01291	0.2796	0.0127	4.117E-16	Yes
0.0331	0.3478	16.79	0.01293	0.2796	0.0127	4.117E-16	Yes

Trajectory of different particles can be obtained by plotting Rpar vs. Lpar, shown in Figure 47.

Rpar means the length of particle travels in radius direction from the center of tube separator.

Lpar indicates the how far it goes from the entrance of the separator.

Figure 47: Trajectory of 3 micron particle
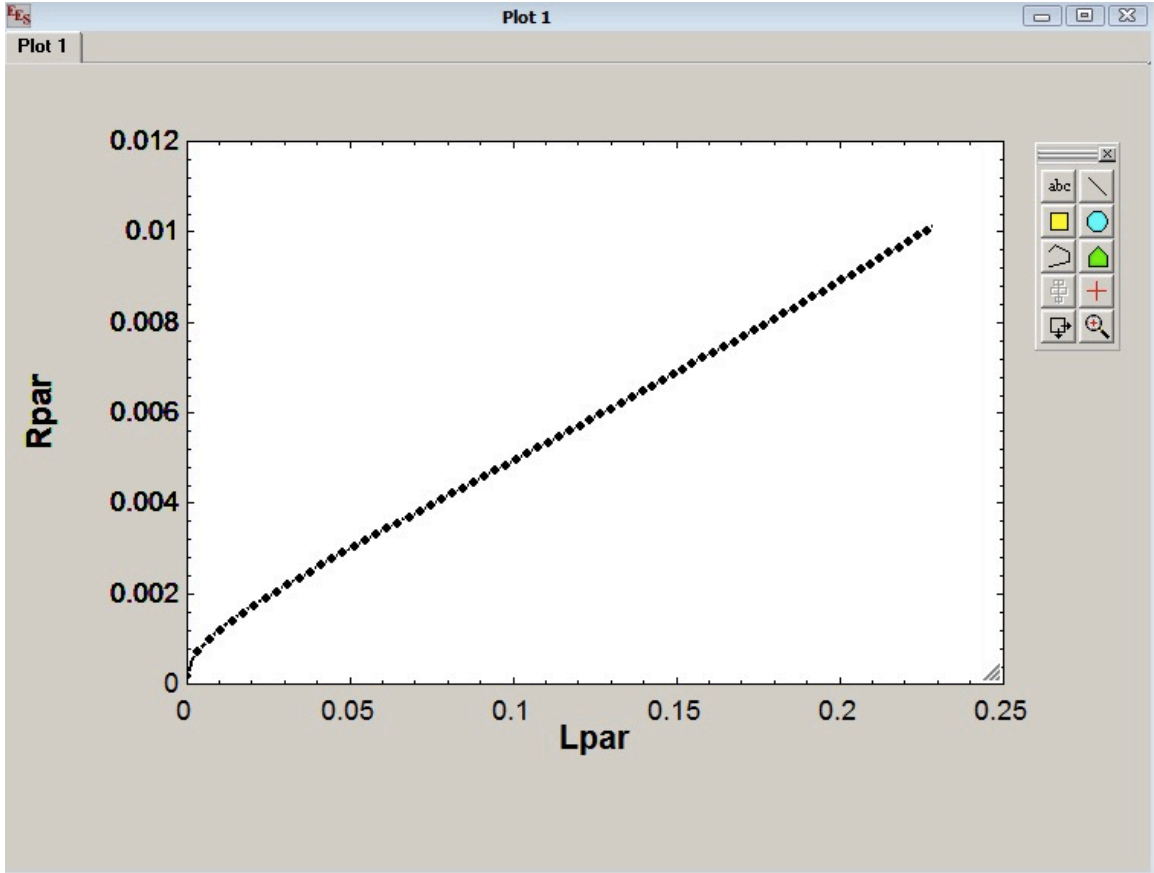
Table 6 shows parametric study for 3 micron particle. Ri indicates the initial position of the

particle. If the "Collect$" column shows "No", it means that particles entering the separator at

corresponsive initial location Ri cannot be collected by the separator. So for particles with 3

micron, it can be collected at initial location 0.001925m from the center of separator. It indicates

that a ratio of 97.71% of the particles can be collected.

Table 6: Parametric study for 3 micron particles

Run	Ri	Ratio	Collect$
1	0.00015	100	No
2	0.0002768	99.96	No
3	0.0004035	99.91	No
4	0.0005303	99.83	No
5	0.0006571	99.74	No
6	0.0007838	99.63	No
7	0.0009106	99.49	No
8	0.001037	99.34	No
9	0.001164	99.17	No
10	0.001291	98.97	No
11	0.001418	98.76	No
12	0.001544	98.53	No
13	0.001671		
14	0.001798		
15	0.001925	97.71	Yes
16	0.002052	97.4	Yes
17	0.002178	97.07	Yes
18	0.002305	96.71	Yes
19	0.002432	96.34	Yes
20	0.002559	95.95	Yes
21	0.002685	95.54	Yes
22	0.002812	95.1	Yes
23	0.002939	94.65	Yes
24	0.003066	94.18	Yes
25	0.003192	93.69	Yes
26	0.003319	93.18	Yes
27	0.003446	92.64	Yes
28	0.003573	92.09	Yes
29	0.003699	91.52	Yes
30	0.003826	90.93	Yes
31	0.003953	90.32	Yes
32	0.00408	89.69	Yes
33	0.004207	89.04	Yes
34	0.004333	88.36	Yes
35	0.00446	87.67	Yes
36	0.004587	86.96	Yes
37	0.004714	86.23	Yes
38	0.00484	85.48	Yes
39	0.004967	84.71	Yes
40	0.005094	83.92	Yes
41	0.005221	83.11	Yes
42	0.005347	82.28	Yes
43	0.005474	81.43	Yes
44	0.005601	80.56	Yes
45	0.005728	79.67	Yes
46	0.005855	78.75	Yes
47	0.005981	77.82	Yes

48	0.006108	76.87	Yes
49	0.006235	75.9	Yes
50	0.006362	74.91	Yes
51	0.006488	73.9	Yes
52	0.006615	72.87	Yes
53	0.006742	71.82	Yes
54	0.006869	70.75	Yes
55	0.006995	69.66	Yes
56	0.007122	68.55	Yes
57	0.007249	67.43	Yes
58	0.007376	66.28	Yes
59	0.007503	65.11	Yes
60	0.007629	63.92	Yes
61	0.007756	62.71	Yes
62	0.007883	61.48	Yes
63	0.00801	60.23	Yes
64	0.008136	58.96	Yes
65	0.008263	57.67	Yes
66	0.00839	56.36	Yes
67	0.008517	55.03	Yes
68	0.008643	53.68	Yes
69	0.00877	52.32	Yes
70	0.008897	50.93	Yes
71	0.009024	49.52	Yes
72	0.009151	48.09	Yes
73	0.009277	46.64	Yes
74	0.009404	45.17	Yes
75	0.009531	43.68	Yes
76	0.009658	42.18	Yes
77	0.009784	40.65	Yes
78	0.009911	39.1	Yes
79	0.01004	37.53	Yes
80	0.01016	35.94	Yes
81	0.01029	34.34	Yes
82	0.01042	32.71	Yes
83	0.01054	31.06	Yes
84	0.01067	29.39	Yes
85	0.0108	27.71	Yes
86	0.01093	26	Yes
87	0.01105	24.27	Yes
88	0.01118	22.52	Yes
89	0.01131	20.76	Yes
90	0.01143	18.97	Yes
91	0.01156	17.16	Yes
92	0.01169	15.33	Yes
93	0.01181	13.49	Yes
94	0.01194	11.62	Yes
95	0.01207	9.733	Yes
96	0.01219	7.827	Yes

97	0.01232	5.9	Yes
98	0.01245	3.953	Yes
99	0.01257	1.987	Yes
100	0.0127	-1.193E-16	Yes

Varialbles [electric field and charge density]:

syms C1 C2 per Current Length J J0 RD IM Rwire Dwire Rcylinder Vwire Vcylinder Emax

Variables [Trajectory of droplets]:

P stands for particles, that is, droplets

syms Up U Fd Fe g RhoP RhoA Qfld RP Dp Ke Cd Re u g Time

Boundary Conditions

Rwire=0.022/2*10^(-2);

Dwire=2*Rwire*100;

Rcylinder=1.7/2*10^(-2);

Vwire=7500;

Vcylinder=0;

Parameters

% Permittivity

per=8.85418781762*10^(-12);

% Relative Density [Unit: T: K, P: mmHg]

T0=298;

P0=760;

T=298;

P=760;

RD=T0/T*P/P0;

% Ion Mobility

IM=1.5*10^(-4);

% Current Density

Current=0.63*10^(-3);

Length=25*10^(-2);

J=Current/Length

J =

0.0025

Threshold Field Strength

Emax=(30*RD+9*(2*RD/Dwire)^0.5)*10^5

Emax =

1.1581e+07

Equations to calculate C1 and C2

% Equation Criteria,Current Density

% Average Electric Field

Ea=Vwire/(Rcylinder-Rwire)

J0=[18]^2*2*pi*per*IM;

[C1, C2]=

solve((J/(2*3.14159*per*IM)*Rwire^2+C1)^.5+C1^.5*log(((J/(2*3.14159*per*IM)___

Ea =

8.9392e+05

C1 =

1279396.028041837613734648790520

C2 =

-10414.890634522985224925251657637

Electric Field

r is the distance from random point to wire

E=(J/(2*pi*per*IM)+C1/r^2)^.5

E0=(J/(2*pi*per*IM)+C1/Rwire^2)^.5;

E0=double(E0)

ezplot(E, [Rwire, Rcylinder])

xlabel('Distance r (m)')

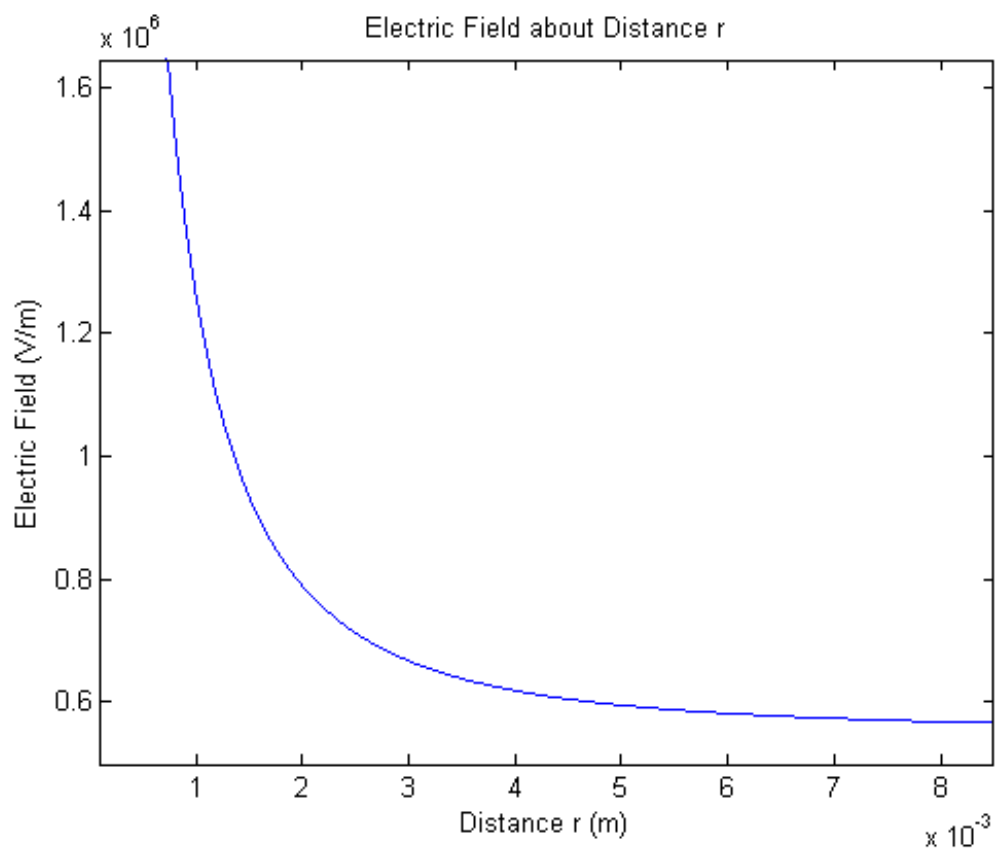ylabel('Electric Field (V/m)')

title('Electric Field about Distance r')

E =

(1279396.0280418376137346487905209/r^2 +

4947668829070689/16384)^(1/2)

E0 =

1.0297e+07

Charge Density

q=J/(2*pi*r*IM*E)

ezplot(q, [Rwire, Rcylinder])

xlabel('Distance r (m)')

ylabel('Charge Density (C/m^3)')

title('Charge Density about Distance r')

q =42/(5*pi*r*(1279396.0280418376137346487905209/r^2 +

4947668829070689/1638▮▮
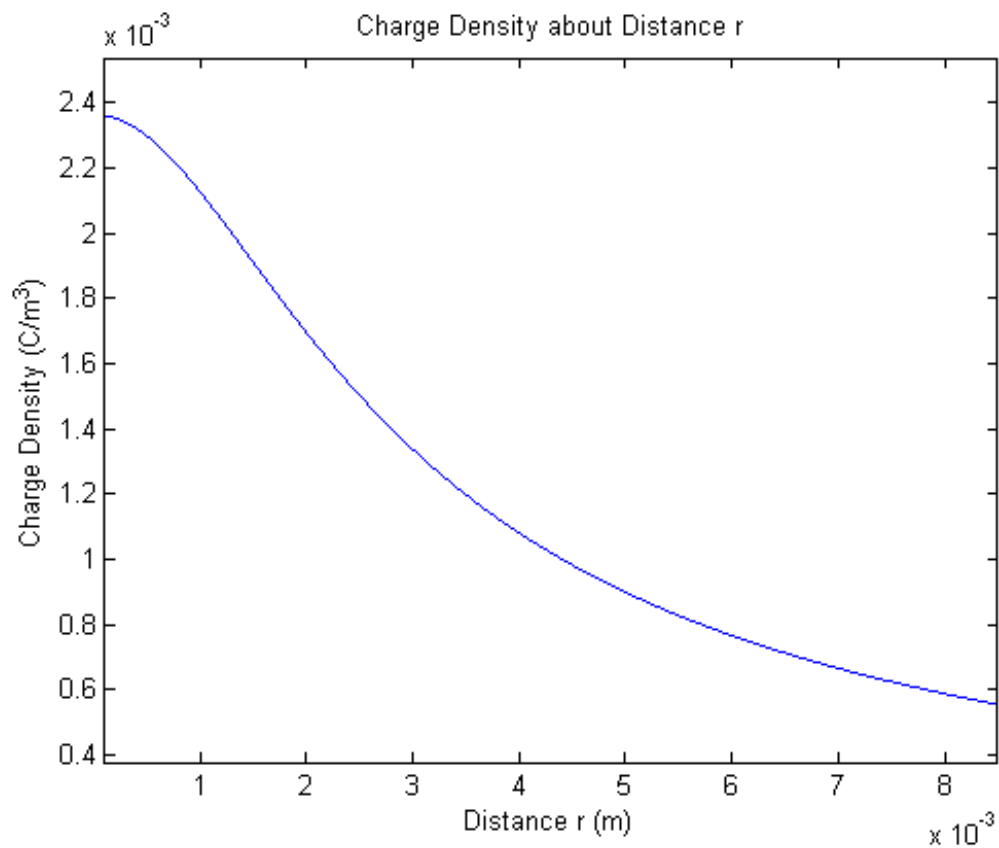
Voltage

Voltage=

-(J/(2*3.14159*per*IM)*r^2+C1)^.5+C1^.5*log(((J/(2*3.14159*per*IM)*r^2+C1)^.▮▮
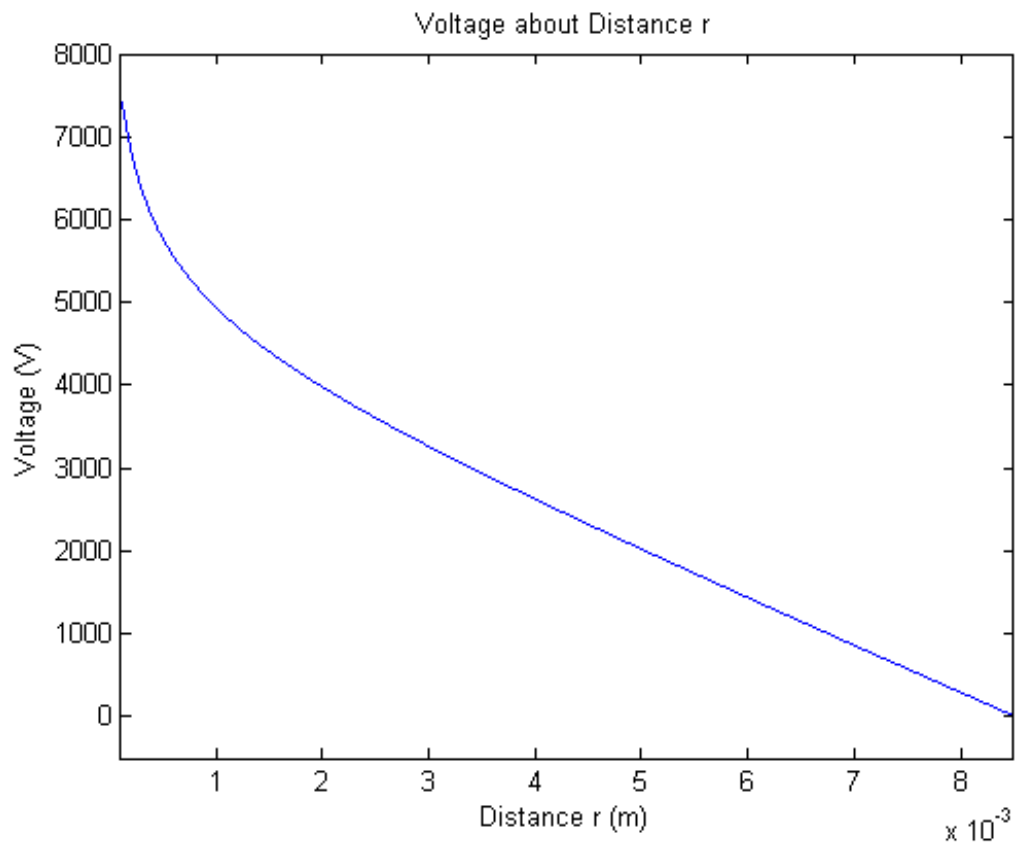
ezplot(Voltage, [Rwire, Rcylinder])

xlabel('Distance r (m)')

ylabel('Voltage (V)')

title('Voltage about Distance r')

Parameters:

Relative permittivity of a particle, use water at 20 C

RP=80;

% Ke: Proportionality constant 9.0*10^9 [N*m^2/C^2]

Ke=9.0*10^9;

% Droplets size [m]

Dp=2*10^(-6);

% Density of air [kg/m^3] at 25 C

RhoA=1.1839;

% Density of droplets [kg/m^3]

RhoP=1000;

% Fluid Viscosity [N*s/m^2=kg/ms] at 25 C

u=1.983*10^(-5);

% Fluid velocity m/s

U=10;

% acceleration due gravity [m/s2]

g=9.8;

% Total Particle Charge

% Assume no diffusion charging, because the particle size is over 1 um

% Field Charging

Qfld=3*RP/(RP+2)*Emax*Dp^2/(4*Ke);

% Electrostatic body force exerted on a charged aerosol

Fe=Qfld*Emax/(1/6*pi*Dp^3*RhoP);

Trajectory of particle

Cd = 24/Re Re=0-0.1; Cd = 22.73/Re-0.0903/Re^2+3.69 Re=0.1-1; Cd = 29.1667/Re-3.8889/Re^2+1.222

Re=1-10; Cd = 46.5/Re-116.67/Re^2+0.6167 Re=10-100;

[Up, Re, Cd]= solve(Re-RhoA*Dp*(Up-U)/u, (Cd*Re/24*18*u/(RhoP*Dp^2))*(U-Up)+g*(RhoP-% Stokes drag term

% Reynolds number

% Re=RhoA*Dp*(Up-U)/u

% Cd: Drag coefficient

% Fd=Cd*Re/24*18*u/(RhoP*Dp^2);

Re=double[18]

Up=double(Up)

Cd=double(Cd)

Re =

                    8.5417

                    -32.4097

        Up =

                    4.5833

0.3184

Cd =

81.5356

-261.4268

Residual time

Time=Length/U

Time =

0.0250

Nomenclature

C_D	Drag coefficient
d_c	cylinder diameter (m)
D_{Ndrop}	number median droplet diameter (cm)
d_p	diameter of particle (m)
d_W	diameter of wire (m)
E	electric field strength (V/m)
E_0	initial field strength (V/m)
F	crystal frequency (Hz)
F_e	electrostatic body force (N/m2)
F_D	Stocks drag term (s^{-1})
J	current density (A/m^3)
g	acceleration due to gravity (m/s^2)
K_E	proportionality constant ($9.0*10^9$ N*m^2/C^2)
P	actual fluid pressure (mm)
P_0	normal atmosphere pressure (mm)
q_{diff}	charge on a particle due to diffusion charging (C)
q_{fld}	charge on a particle due to field charging (C)
q_p	charge on a particle due to diffusion and filed chagrin (C)
Re	Reynolds number
S	liquid surface tension(dynes/cm)
t	resident time(s)
T	Actual fluid temperature (K)
T_0	Absolute ambient temperature (K)

u	velocity of airflow (m/s)
u_p	velocity of particles (m/s)
Z_i	ion mobility (m^2/(V*s)
ϕ	electrical potential (V)
μ	fluid viscosity
δ	relative density
ε_p	relative permittivity of particles
ρ	liquid density
ρ_a	density of airflow (kg/m3)

Bibliography

[1]   K. R. Parker and E. Institution of Electrical, *Electrical operation of electrostatic precipitators*: Institution of Electrical Engineers, 2003.

[2]   C.-C. Sung, C.-Y. Bai, J.-H. Chen, and S.-J. Chang, "Controllable fuel cell humidification by ultrasonic atomization," *Journal of Power Sources,* vol. 239, pp. 151-156, 10/1/ 2013.

[3]   C. Rodes, T. Smith, R. Crouse, and G. Ramachandran, "Measurements of the Size Distribution of Aerosols Produced by Ultrasonic Humidification," *Aerosol Science and Technology,* vol. 13, pp. 220-229, 1990/01/01 1990.

[4]   K. Teschke, Y. Chow, C. Netten, S. Varughese, S. M. Kennedy, and M. Brauer, "Exposures to Atmospheric Effects in the Entertainment Industry," *Journal of Occupational and Environmental Hygiene,* vol. 2, pp. 277-284, 2005/05/01 2005.

[5]   D. Mondal, A. Datta, and A. Sarkar, "Droplet size and velocity distributions in a spray from a pressure swirl atomizer: application of maximum entropy formalism," *Proceedings of the I MECH E Part C Journal of Mechanical Engineering Science,* vol. 218, pp. 737-749, 2004.

[6]   P. E. Santangelo, "Characterization of high-pressure water-mist sprays: Experimental analysis of droplet size and dispersion," *Experimental Thermal and Fluid Science,* vol. 34, pp. 1353-1366, 11// 2010.

[7]   S. Yoon, D. Kim, D. Kim, and B. Kim, "Effect of nozzle geometry for swirl type twin-fluid water mist nozzle on the spray characteristic," *Journal of Mechanical Science and Technology,* vol. 25, pp. 1761-1766, 2011/07/01 2011.

[8]   A. Farnoud and E. Southern Methodist University. Environmental and Civil, *Electrostatic Removal of Diesel Particulate Matter*: Southern Methodist University, 2008.

[9]   S. American Chemical, *Chemical Abstracts*: American Chemical Society., 1911.

[10]   C. Yi, P. Dou, C. Wu, H. Ou, W. Qu, and S. Ma, "Experimental study of transportion characteristic of charged particle in a laboratory scale high velocity electrostatic precipitator," in *Mechanic Automation and Control Engineering (MACE), 2010 International Conference on*, 2010, pp. 2038-2042.

[11]   A. Bologa, A. Hornung, H. Seifert, K. Woletz, and H. R. Paur, "Application of space-charge electrostatic precipitator for collection of oil mist from pyrolysis gases," in *Dielectric Liquids, 2008. ICDL 2008. IEEE International Conference on*, 2008, pp. 1-4.

[12]   J. Podlinski, A. Niewulis, V. Shapoval, and J. Mizeraczyk, "Electrohydrodynamic secondary flow and particle collection efficiency in a one-sided spike-plate type electrostatic precipitator," *Dielectrics and Electrical Insulation, IEEE Transactions on,* vol. 18, pp. 1401-1407, 2011.

[13]   P. J. McKinney and J. H. Davidson, "Particle motion in a barbed plate electrostatic precipitator," in *Industry Applications Society Annual Meeting, 1994., Conference Record of the 1994 IEEE*, 1994, pp. 1505-1512 vol.2.

[14]   N. Grass, W. Hartmann, and M. Klockner, "Application of different types of high voltage supplies on industrial electrostatic precipitators," in *Industry Applications Conference, 2002. 37th IAS Annual Meeting. Conference Record of the*, 2002, pp. 270-276 vol.1.

[15]   L. M. Dumitran, P. Atten, D. Blanchard, and P. Notingher, "Drift velocity of fine particles estimated from fractional efficiency measurements in a laboratory-scaled electrostatic precipitator," *Industry Applications, IEEE Transactions on,* vol. 38, pp. 852-857, 2002.

[16]   S. Touhami, W. Aksa, K. Medles, A. Tilmatine, and L. Dascalescu, "Numerical simulation of the trajectories of insulating particles in a tribo-aero-electrostatic separator," in *Industry Applications Society Annual Meeting, 2014 IEEE*, 2014, pp. 1-6.

[17]   B. S. Rajanikanth and B. R. Prabhakar, "Modeling of prebreakdown VI characteristics of a wire-plate electrostatic precipitator operating under combined dc-pulse energization," *Dielectrics and Electrical Insulation, IEEE Transactions on,* vol. 1, pp. 1058-1067, 1994.

[18]   Q. Lancereau, J. M. Roux, and J. L. Achard, "Electrohydrodynamic flow regimes in a cylindrical electrostatic precipitator," *Dielectrics and Electrical Insulation, IEEE Transactions on,* vol. 20, pp. 1409-1420, 2013.

[19]   Z.-j. Ding, L. Xiao, and L.-c. Xiao, "Experimental Study on V-I Characteristics of Wet Electrostatic Precipitator," in *Intelligent Computation Technology and Automation (ICICTA), 2012 Fifth International Conference on*, 2012, pp. 170-172.

[20]   B. Chua, A. S. Wexler, N. C. Tien, D. A. Niemeier, and B. A. Holmen, "Collection of Liquid Phase Particles by Microfabricated Electrostatic Precipitator," *Journal of Microelectromechanical Systems,* vol. 22, pp. 1010-1019, Oct 2013.

[21]   T. Yamamoto, T. Abe, T. Mimura, N. Otsuka, Y. Ito, Y. Ehara*, et al.*, "Electrohydrodynamically-Assisted Electrostatic Precipitator for Collection of Low Resistive Dust," in *Industry Applications Society Annual Meeting, 2008. IAS '08. IEEE*, 2008, pp. 1-5.

[22]   A. Zukeran, Y. Ikeda, Y. Ehara, M. Matsuyama, T. Ito, T. Takahashi*, et al.*, "Two-stage-type electrostatic precipitator re-entrainment phenomena under diesel flue gases," *Industry Applications, IEEE Transactions on,* vol. 35, pp. 346-351, 1999.

[23]   A. J. Schwab, "Local occurrence of back corona at the dust layer of electrostatic precipitators," in *Electrical Insulation and Dielectric Phenomena, 2000 Annual Report Conference on*, 2000, pp. 93-96 vol.1.

[24]   W. Xiaohua and Y. Changfu, "Effect of humidity on negative corona discharge of electrostatic precipitators," *Dielectrics and Electrical Insulation, IEEE Transactions on,* vol. 20, pp. 1720-1726, 2013.

[25]   J. S. Chang, J. Dekowski, J. Podlinski, D. Brocilo, K. Urashima, and J. Mizeraczyk, "Electrohydrodynamic gas flow regime map in a wire-plate electrostatic precipitator," in *Industry Applications Conference, 2005. Fourtieth IAS Annual Meeting. Conference Record of the 2005*, 2005, pp. 2597-2600 Vol. 4.

[26]   O. Blejan, P. V. Notingher, L. M. Dumitran, M. Younes, A. Samuila, and L. Dascalescu, "Experimental Study of the Corona Discharge in a Modified Coaxial Wire-Cylinder Electrostatic Precipitator," *Industry Applications, IEEE Transactions on,* vol. 46, pp. 3-8, 2010.

[27]   A. Mizuno, "Electrostatic precipitation," *Dielectrics and Electrical Insulation, IEEE Transactions on,* vol. 7, pp. 615-624, 2000.

[28]   M. Alshehhi, A. Shooshtari, S. Dessiatoun, M. Ohadi, and A. Goharzadeh, "Parametric Performance Analysis of an Electrostatic Wire-Cylinder Aerosol Separator in Laminar Flow Using a Numerical Modeling Approach," *Separation Science and Technology,* vol. 45, pp. 299-309, 2010/02/19 2010.